# POLITECNICO DI TORINO

Master of Science Program
in AUTOMOTIVE ENGINEERING

Master Degree Thesis

# Design of a Battery Pack for a Formula SAE Racing Car



**Supervisor**
Prof. Andrea Tonoli

**Candidate**
Francesco Leotta

Academic Year 2019/2020

# Contents

# List of Figures

# List of Tables

# List of Acronyms

**AIR**  Accumulator Isolation Relay

**B-EMF**  Back Electromotive Force

**BOM**  Bill of Material

**BMS**  Battery Management System

**CFD**  Computational Fluid Dynamics

**CID**  Current Interrupt Device

**CPU**  Central Processing Unit

**CV**  Combustion Vehicles

**DV**  Driverless Vehicles

**EV**  Electric Vehicles

**IMD**  Insulation Monitoring Device

**NTC**  Negative Thermal Coefficient

**PCB**  Printed Circuit Board

**PTC**  Positive Thermal Coefficient

**RMS**  Root Mean Square

**SAE**  Society of Automotive Engineers

**SOC**  State of Charge

**TSAL**  Tractive System Active Light

# Abstract

The present thesis is the result of my work in Squadra Corse PoliTo during the 2018/19 season. The aim of this project is to describe the passages to design the battery pack for the SC19, the racing car which participated in the Formula SAE competition in the 2019's summer.

The thesis begins with an overview of the race and the team, aimed at illustrating the environment in which the design was carried out. The goals, the structure and every event of the competition are described to clarify the mission that the battery pack has to accomplish.

The first part is about the target setting concerning each aspect of the battery pack. The influence of different assemblies of the car is considered, as well as the data collected in previous years and the comparison with the competitors. Moreover, the main constraints introduced by the competition rules are taken into account.

In 2018 the team decided to adopt a Lithium-ion battery. This was a solution different in chemistry and shape from the previous years. The reasons why this change was confirmed in 2019 are explained. Different batteries with their configuration are then analysed.

The work proceeds describing the thermal management system. It begins with the analysis of the previous season's cooling system, followed by the optimization of individual cooling components. Track tests and bench tests representative of the working conditions are reported.

The packaging of all the components belonging to the battery pack is presented. In detail, the module design, considering electrical connections and sensor positioning, is illustrated.

The thesis concludes with the description of the procedures to produce the accumulator container and cover, starting from the material choice and ending with the mould design and the final handmade production.

# Chapter 1

# Introduction

## 1.1   Formula SAE

The Formula SAE is a competition that allows students, coming from all over the world, to go beyond the theory learned at school, involving them in a more practical way. Each team that participates has create a small formula-style vehicle, i.e. open-wheeled, single-seat and open cockpit, from the concept to the final production. The entire process must be done without involvement of professional figures. The competition is split into the following classes:

- Internal Combustion Engine Vehicles (CV)

- Electric Vehicles (EV)

- Driverless Vehicles (DV)

The car design must be carried out keeping into consideration all the rules relative to the class to which it belongs.

The competition is divided into three main sections: the technical inspection, the static events and the dynamic events.

The design of the car is therefore influenced and constrained by the rules and by the variety of events to which it has to participate. All the aspects related to the competitions and to the rules, resumed in the next pages, are explained in a more detailed way in the document published by SAE International [1].

### 1.1.1 Technical inspection

The competition starts with a series of technical inspections to check the vehicle for safety and compliance with the rules. For what concerns the EV, the technical inspection is divided into the following parts:

- Pre-inspection: drivers' equipment, safety equipment (fire extinguishers), rims and tires (both for dry and wet conditions) are checked.

- Accumulator inspection: the compliance of the accumulator to the rules is verified. The accumulator insulation and the data acquisition method are tested. Also the accumulator related equipment such as gloves, hand cart for transportation and charger are checked. After this inspection the accumulator is sealed for the rest of the competition.

- Electrical inspection: all the electrical components are checked, including the electronic boards and every datasheet. The insulation of the whole vehicle is then tested in different points of the car.

- Mechanical inspection: the measures that the car has to satisfy are checked. During this inspection all the samples tested for the chassis strength and for the impact attenuator must be shown. Finally the equipment to push and to lift the car is tested.

- Tilt test: the vehicle is placed on a tilt table which is tilted to an angle of 60° as shown in *figure 1.1a*. It is conducted with the tallest driver seated in the normal driving position and with all vehicle fluids at their maximum level. In order to pass the test, the car must remain in contact with the tilt table and, at the same time, there must be no fluid leaking.

- Vehicle weighing: just for annotating the car weight.

- Rain test: all the components used to avoid the water entering into the vehicle are tested as shown in *figure 1.1b*. The car must be switched on during the test. A large amount of water is directed towards the vehicle for 120 s to simulate heavy rain conditions. The device monitoring the insulation must not detect humidity for the entire duration of rain simulation, plus other 120 s from the interruption of water spraying.

(a) Tilt                                                   (b) Rain

Figure 1.1: Technical Inspection

- Brake test: the aim of the test is to verify the efficiency of the mechanical brakes, especially in electric cars which use regenerative braking. The driver must accelerate the car, switch off the tractive system and brake the car within certain limits. The wheels must lock and the car must follow a straight line. All the lights related to braking and tractive system are also checked during the test.

The car must pass all the technical inspections before taking part in the dynamics events.

## 1.1.2 Static Events

The static events take place concomitantly with the technical inspection. In this phase the team has to show to the judges the car from a theoretical point of view, illustrating the design process followed, the organization of the team and the fictitious idea of business.

The static events are therefore divided into three categories:

- Business plan presentation: during this speech the judges, in this case economists, behave like potential investors looking for new opportunities. The team has to present its product, a prototype vehicle, pretending to be a real enterprise. The aim is to create a complete business model, making a detailed plan of the investments needed to start a mass production of the vehicle and foreseeing the

profitability of it in different scenarios. In the end, a score will be assigned, taking into account the detail level of the business plan and the originality of the idea.

- Cost and manufacturing: all the documentation about the organization of the team, collected during the entire project, is evaluated. The team has to present an Engineering BOM and a Manufacturing BOM and has to provide all the information about the costs of materials, components, processes and so on. In addition, the make or buy decisions must be highlighted and explained. Also in this case a score is given, considering the level of detail and evaluating the cost understanding.

- Engineering design: the aim of this event is to evaluate the design process at every stage, from the concept and simulation, to the realization and validation. Each department of the team has to show, explain and justify all the choices taken and has to answer to the judges' questions. The most important thing is not to have the best technology but to exploit in the best way the resources available. This is the reason why the knowledge and the awareness about the work carried out, in the field of competence, are evaluated. Among the three static events, this is the one which is worth the most.

The score achievable with the static events are summarized in *table 1.1*.

| Static event | Points |
| --- | --- |
| Business plan presentation | 75 |
| Cost and manufacturing | 100 |
| Engineering design | 300 |

Table 1.1: Static events score

### 1.1.3 Dynamic Events

The objective of the dynamic events is to evaluate the car performances relatively to the vehicles of the other teams. The point system is made in such a way that the fastest

car takes the maximum points available for that particular event, while the other participants take a number of points scaled relatively to the best time registered. The scores assigned to the best performances are summarized in *table 1.2*.

| Dynamic event | Points |
|---|---|
| Skidpad | 75 |
| Acceleration | 75 |
| Autocross | 100 |
| Endurance | 325 |
| Efficiency | 100 |

Table 1.2: Dynamic events score

The dynamic events are divided in this way:

- Skidpad: the track is made of two identical circles constituting an eight pattern as shown in *figure 1.2*.
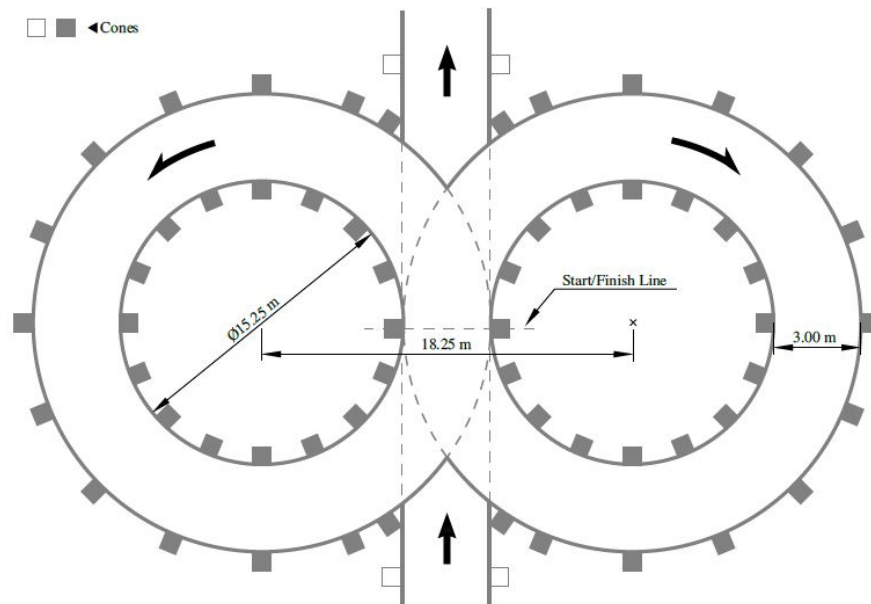


Figure 1.2: Skidpad track [1]

5

The mean diameter of the circle is 18,25 m and the lane is 3 m wide. The line passing through the centres of the circles defines the starting line and at the same time the finishing line. The car enters perpendicularly to the eight pattern and then takes two laps on the right circle and other two on the left circle. The first and third laps are not recorded, they are aimed at preparing the second and the fourth laps that are instead recorded. The run time is the average time between the second and the fourth laps plus eventual penalties.

- Acceleration: the track is a simple straight line 75 m long and 5 m wide. The starting is from standstill.

- Autocross: the track is a mixed one (straights, turns and slaloms) and its length is below 1,5 km. The straights cannot be longer than 80 m, the minimum track width is 3 m and the space between two consecutive cones of a slalom is between 7,5 m and 12 m. This event foresees only one lap.

- Endurance: the track layout is similar to the autocross track. In this case, more laps must be completed for a total length of about 22 km. During the endurance there is only one stop period 180 s long halfway through the race, in which it is not possible to recharge the battery (in case of EV). Wheel-to-wheel racing with other cars is not allowed, so the overtaking manoeuvres are driven by flags.

- Efficiency: this is not a separate event but it is part of the endurance. The aim is to evaluate how efficiently the car has completed the whole endurance. The energy regenerated is multiplied by a factor of 0,9 and it is subtracted to the energy spent during the battery discharging.

## 1.2 Squadra Corse Polito

Squadra Corse PoliTo is the team established in 2004 at Politecnico di Torino, whose objective is to design and build, year by year, a prototype racing car competing in Formula SAE. The team is based in Mirafiori Campus, where all the design related activities are carried out, while the assembly and manufacturing operations have as main site the FCA Prototypes plant.

Figure 1.3: SC19 racing car

The first cars produced were equipped with internal combustion engines, but in 2012 the team decided to leave this solution to follow the electrification trend. From that year, Squadra Corse PoliTo started producing racing cars powered by electric powertrains.

During the years, hundreds of students passed through the team, giving their contribution and receiving knowledge and experience in return. Thanks to them, the cars conceived followed a constant growth, passing from a tubular steel frame to a modern monocoque entirely made of carbon fibre, adding an aerodynamics package not present at the beginning, developing some interesting and fundamental tools like the lap time simulator and tuning all the other components trying to be always aligned with the state of the art. All these factors have led to the 2019's car called SC19 shown in *figure 1.3*.

The team is organized in divisions, each headed by a responsible. They are in turn managed by a technical director and a team leader. Each division takes care of one assembly of the car and they are:

- Aerodynamics: in charge of developing the aerodynamics package. The SC19 is equipped with front and rear wings, undertray, diffuser and sidepods, all made of

carbon fibre. Thanks to them the car can generate more than 500 N of downforce, balanced 50%-50% between the two axles, limiting the drag and ensuring an efficiency of about 4.

- Battery Pack: the accumulator is entirely made by the team except for the BMS that is supplied and customized by a partner company. It consists of Li-ion cylindrical cells arranged in 4p-140s layout air-cooled. The energy stored is equal to 6,2 kWh and the maximum voltage is 588 V. The accumulator case is made of carbon fibre to reduce the weight as much as possible.

- Chassis: the monocoque is made of sandwich panels of carbon fibre and honeycomb core. They ensure a low weight (below 20 kg) and a high torsional stiffness (above 203000 Nm/rad). The division is also responsible for the ergonomics.

- Electric and electronics: almost all the printed circuit boards are designed by the division. It is also in charge of the wiring harness.

- Management: this division manages the team from a logistic point of view and has to prepare all the material necessary for the competition in addition to the business plan.

- Powertrain: the SC19 is equipped with 4 electric motors, each one is able to provide 35 kW of peak power, 21 Nm of torque and 20000 rpm. The epicyclic gear train then can reduce the speed and increase the torque by guaranteeing a gear ratio equal to 14,5:1. The division also takes care of the cooling of motors and inverters.

- Unsprung masses: this division is in charge of the brake system, the steering system and the suspension system. The suspension system is composed of a double wishbone architecture with anti-roll bar, hydraulic damper and an air spring. The vehicle is equipped with hollow shell A-arms made of carbon fibre reinforced polymer, which have permitted to save more than 50% of mass with respect to the steel ones that have the same stiffness.

- Vehicle dynamics: it occupies about vehicle state estimation, vehicle dynamics controls and power management. The *SC19* uses systems like launch control, traction control, torque vectoring and yaw rate control.

# Chapter 2

# Target setting

To design a battery pack, the first step is to establish the targets and the constraints relative to the project and to the field of application. It is important to not think to the accumulator as a single component, but it is crucial to see it like an assembly belonging to a system. One parameter that would seem beneficial for the battery pack could be disadvantageous for another assembly of the system.This is the reason why, in establishing the targets and the constraints, aspects related to the motors, suspensions, chassis and vehicle dynamics have been considered. In addition to that, the most performant solution could not be the best from the economical point of view or the time point of view. In this field, there is indeed a budget to respect and the whole project from the concept to the realization takes less than 10 months.

Some choices could be based on the availability of specific products or processes. An advanced technology is sometimes available thanks to the partner involved in the projects, however, other times it is necessary to use older and simpler components or technologies.

## 2.1 Energy

The first target was about the energy needed to complete the longest event, which is the endurance. It was 22 km long divided into two stints separated by 180 s of pause. The energy necessary to complete all the laps running at a good pace came from different sources. It was not possible to obtain a precise number because the endurance track

of the different events were not known a priori. For this reason, the energy evaluation was based on simulations, past experiences and benchmarking.

First of all, the lap time simulator was used by the vehicle dynamics division, considering the track layouts of the past years and the different car layouts. The outcome was 425 Wh per lap that, after being multiplied by the number of laps, was 8500 Wh. The energy value obtained was then compared with the real data of the past competitions. One of the events considered was the endurance run in 2018 in Spain. It was representative for the team because all the laps were completed, even if the firsts two laps of the first stint and the first lap of the second stint were performed at low speed because of low driver confidence. The time and the energy spent by the SC18 in each lap are reported in *figure 2.1*. The best lap lasted 72,3 s and the highest consumption registered in one lap was 321,4 Wh, while the mean time was 77,24 s and the mean consumption per lap was 269 Wh.
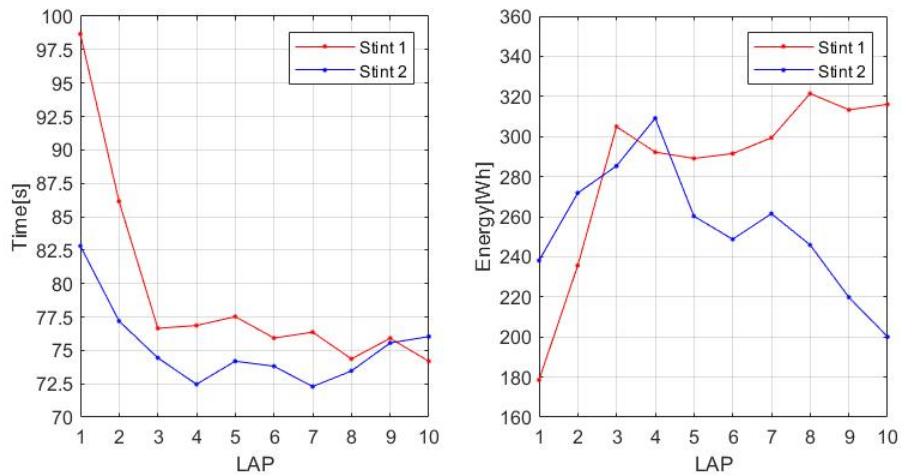


Figure 2.1: Endurance FSS 2018: SC18 time and energy per lap

The comparison with the competitors is shown in *figure 2.2*. The mean energy used per lap by the SC18 was much lower since some overheating problems forced the car to go slower than the others. The best time recorded by the SC18 was indeed lower than the mean time of the first eight best teams. From the benchmarking it was evident how the values registered in Spain with the *SC18* could not be used as direct reference for the energy target. For this reason, it was decided to take as reference the energy of the best teams that matched with the data obtained by the lap time simulator. At the
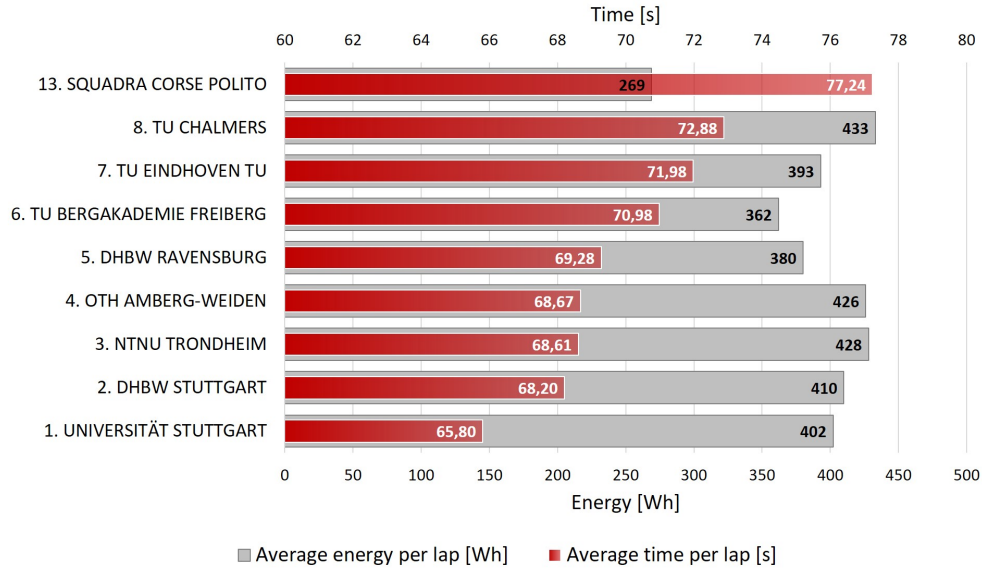
Figure 2.2: Endurance FSS 2018: best competitors benchmarking

energy obtained was then added an additional amount sufficient for ensuring an extra lap. The resulting energy was equal to 8925 Wh, which rounded led to the final energy target of 9000 Wh.

The energy needed to complete the endurance should be provided by the accumulator considering both the energy stored and the regenerated one. The latter is obtained through regenerative braking, a process which allows recovering part of the kinetic energy lost during the deceleration phase, transforming it back into electrical energy that is then stored in the accumulator [2]. Track tests performed with the SC18 had shown that the percentage of energy recoverable out of an event like endurance was 33% at the worst.

The accumulator mounted on the SC18 had the characteristics illustrated in *table 2.1*. Its nominal energy of 8087 Wh was almost equal to the target of 9000 Wh because there was a lack of knowledge about regenerative braking, indeed it was not used during the 2018's competitions. The target for the accumulator energy of the SC19 was set considering the energy recoverable. Therefore, out of 9000 Wh, the 33% (about 2970 Wh) was supposed to be energy recoverable, while the reminder 67% was supposed to be energy stored in the battery pack. This led to the final energy target for the accumulator of 6030 Wh. Thanks to the regenerative braking application the over

11

| Cell | Sony vtc6 |
|---|---|
| Configuration | 5p-144s |
| Capacity | 15,6 Ah |
| Nominal voltage | 518,4 V |
| Energy | 8087,0 Wh |

Table 2.1: SC18 battery pack characteristics

dimensioning of the old accumulator was avoided. The resultant energy reduction, from the 2018's battery pack to the new 2019's target, was about 25%.

The rules also established a maximum energy per module of 6 MJ, i.e. 1666,7 Wh.

## 2.2 Voltage

The voltage target was decided taking into account the field weakening of the permanent-magnet synchronous servo motors. The results of the bench test on the electric motor used are reported in *figure 2.3*.
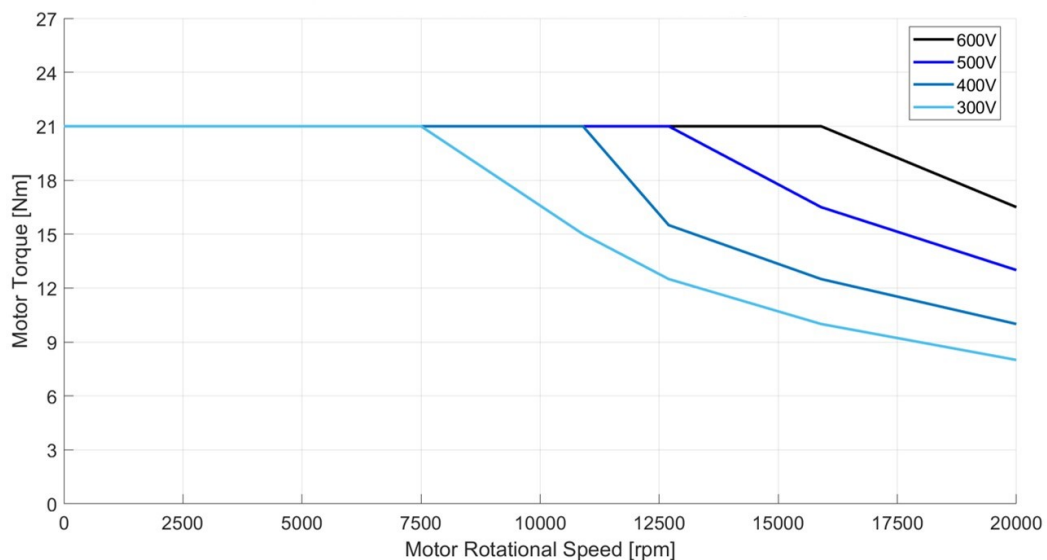


Figure 2.3: Electric motor map

The field weakening due to the B-EMF is shifted at higher motor rotational speed in case of higher battery voltage [3]. The choice of the voltage was based on this consideration, therefore the maximum voltage of 600 V allowed by the rules was taken as target. This allowed to exploit the maximum torque that could be exerted by the motor for a wider range of motor rotational speeds.

The subdivision of the battery pack into modules had to take into account also the maximum voltage allowed by rules of 120 V.

## 2.3  Current

The maximum power that could be exploited was limited by the rules at 80 kW and it was strictly controlled throughout all the dynamic events. The most demanding events for what concerned the power request were the autocross and the acceleration. Both of them are faced with the battery pack fully charged, therefore with a voltage close to the target established before of 600 V. In general, when dealing with cells it is not always possible to reach exactly the voltage desired because of configuration constraints. This is the reason why a lower voltage equal to 580 V was considered in the calculation. The second factor that was taken into account was the voltage drop $\Delta V$ occurring during the current drawing. It can be computed, in first approximation, as shown in *equation 2.1*, where $R$ is the accumulator resistance equal to 0,5 $\Omega$ (value obtained starting from the *SC18* battery pack and rounding up), $P$ is the maximum power equal to 80000 W and $V$ is the open circuit voltage equal to 580 V. The current $I$ can then be computed through the *equation 2.2*.

$$\Delta V = R\,I = R\,\frac{P}{V} = 68,9\,V \tag{2.1}$$

$$I = \frac{P}{V - \Delta V} = 156,5\,A \tag{2.2}$$

Usually, the SOC (State of Charge) is maximum during the autocross and the acceleration. Hence, they are not representative of the worst case scenario. The highest values of current are typically reached during endurance in which the battery pack cannot be recharged, causing the SOC and therefore the voltage to decrease. A decrease in voltage causes an increase in current when the power output is constant, being the

power equal to the product of the voltage and the current. In 2018's battery pack the minimum voltage was 360 V considering the cut-off voltage of the cells used. The minimum voltage in the calculation was set to 350 V also because a lower value would have been too detrimental for the electric motors efficiency. The peak current in low SOC condition with a power equal to 80000 W is shown in *equation 2.3*.

$$I = \frac{P}{V} = 228,6\,A \tag{2.3}$$

This current value has to be divided for the number of parallels of the chosen configuration to find the maximum current passing through a single cell in the worst case scenario (see *figure 2.4*).
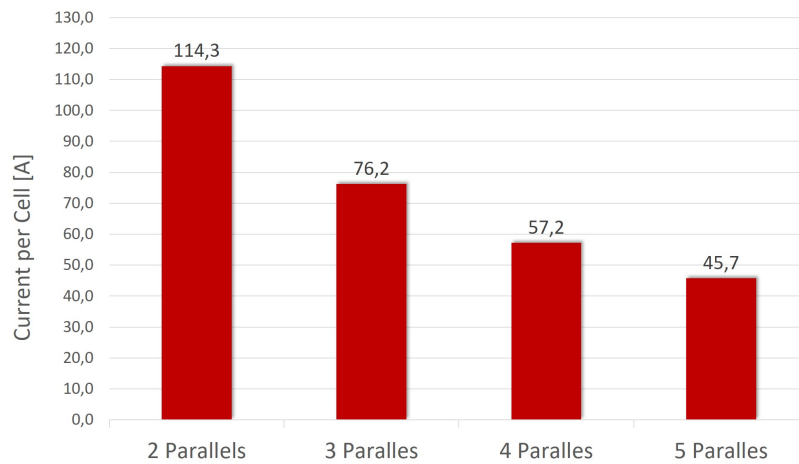


Figure 2.4: Worst case scenario: peak current per cell

As said in chapter 1, the longest straight is 80 m long, which is typically completed in less than 4 s. Therefore, the cell chosen had to withstand the peak current in the worst case for that time interval. In the real case the peak current is usually limited by the BMS, especially in the last laps of the endurance in which the voltage is low. This is done to reduce the stress on the cells, to reduce the power dissipation that is equal to the resistance times the square of the current and to not discharge too quickly the battery.

14

## 2.4 Weight

One of the main objectives was related to the weight reduction. This was the goal for every assembly of the car, including the battery pack. The reduction of weight provides better performance of the vehicle in acceleration, braking and also during cornering thanks to the reduced moments of inertia. In addiction, it allows the reduction of energy consumption, because the weight to accelerate is lower. The weight of 2018 competitor's cars are shown in *table 2.2*.

| Team | Weight |
| --- | --- |
| ETH Zurich | 166 |
| NTNU Trondehim | 183 |
| Running Snail | 202 |
| KIT | 180 |
| TU Eindoven | 197 |
| Monash | 276 |
| Deggendoorf | 193 |
| UAS Nurnberg | 238 |
| TU Delft | 172 |
| TU Munchen | 158 |
| TU Stuttgart | 176 |
| DHBW Stuttgart | 193 |
| Tallin | 184 |
| Global Formula | 190 |
| **Squadra Corse Polito** | **203** |

Table 2.2: 2018 competitors weights

The mean weight was 192,5 kg while the SC18 weight was 203,0 kg so this objective was considered crucial.

A particular target of weight was not set for the battery pack at the beginning of the project, but obviously it was important to not increase it with respect to the SC18 battery pack. The only constraint in terms of weight was established by the rules and

it was 12 kg per module.

Being the battery pack one of the heaviest assemblies (*figure 2.5*), its lightning would have led to a consistent overall weight reduction. Hence, the main objective was to reduce the weight according to the capacity reduction explained before and to better design the internal components of the battery pack to cut out useless weight. This philosophy led also to the use of composite material for the accumulator container, already introduced in 2018.
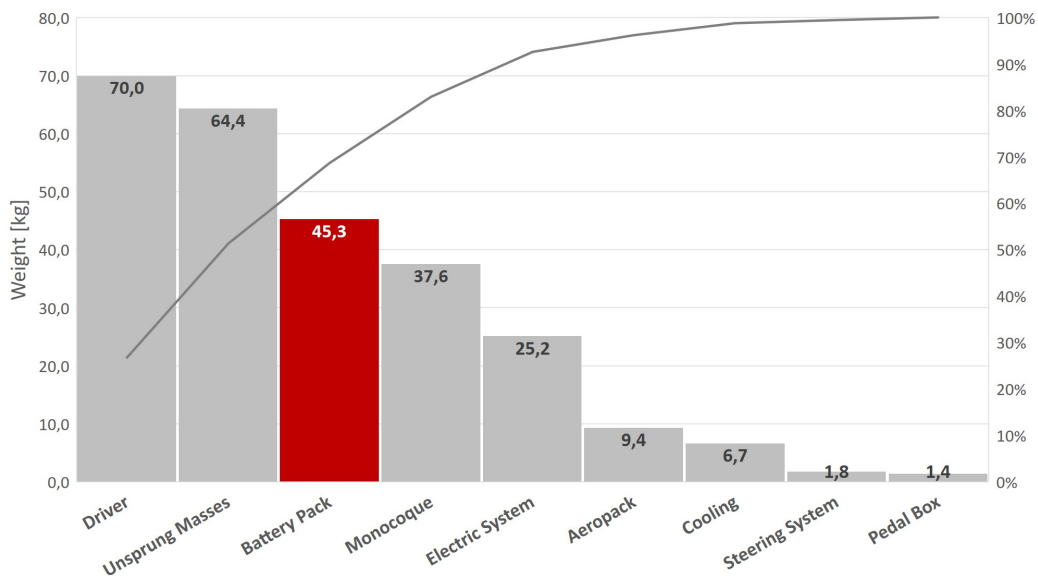


Figure 2.5: SC18 weight distribution

## 2.5 Position and dimensions

The dynamic of the vehicle is strongly influenced by the distribution of the masses. They should be divided between front and rear according to a defined percentage in order to maximize the performance of the car. Moreover, the masses should be as close as possible to the centre of gravity of the car to minimize the moment of inertia around the vertical axis. Another requirement for what concerns mass distribution is to locate them as close as possible to the ground in order to lower the centre of gravity position. This is a main objective in race cars because it allows to reduce the roll motion during

cornering and it allows to lower the car profile, thereby reducing the frontal section (beneficial from an aerodynamic point of view). In the SC19, the weight was divided in the following way: 45% on the front and 55% on the rear. The reduction of the yaw moment of inertia was a primary goal to increase the ease of turning, reduce the understeering behaviour and stabilize the yaw rate controller.

The battery pack was not placed under the floor as in passenger cars because it would have put the driver in a higher position. The driver was much heavier than the battery pack and so he gave the major contribution to the centre of gravity height. For this reason it was preferable to lower his position as much as possible by placing the battery pack in another place. The only available position was in the rear compartment of the car as shown in *figure 2.6*.
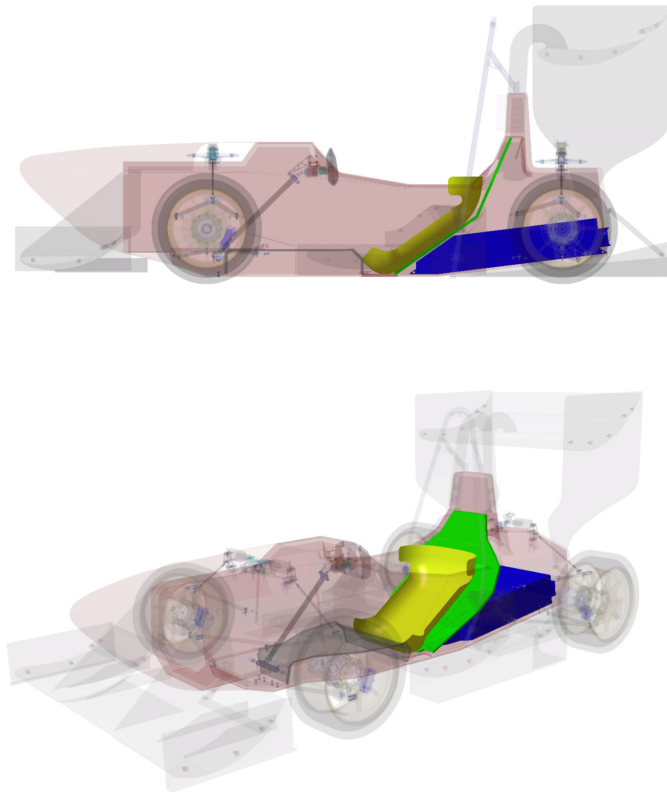
Figure 2.6: Battery pack position

17

In that position, it was as close as possible to the ground but it was not close to the centre of the car. To minimize this drawback, it was chosen to exploit all the space available by placing the front part of the battery pack just under the seat, divided by the firewall (respectively blue, yellow and green in *figure 2.6*).

The positioning of the battery pack inside the car should also satisfy the requirements in terms of maintainability. During the race week the battery pack must be removed several times from the car because it cannot be recharged in the box, but it must be transported in a specific zone. There was thus the necessity to reduce the time to dismount the battery pack. The rear position, already used in the past and confirmed in 2019, facilitated this operation by putting the attachment points in easy accessible points and allowing the removal from the rear opening of the compartment.

The dimensions of the battery pack were subjected to some constraints. The width (length in y-direction) was the main measure to keep within a specific limit. This direction was affected by the arms of the double wishbone suspension. The rear suspension scheme is shown in green in *figure 2.7*.
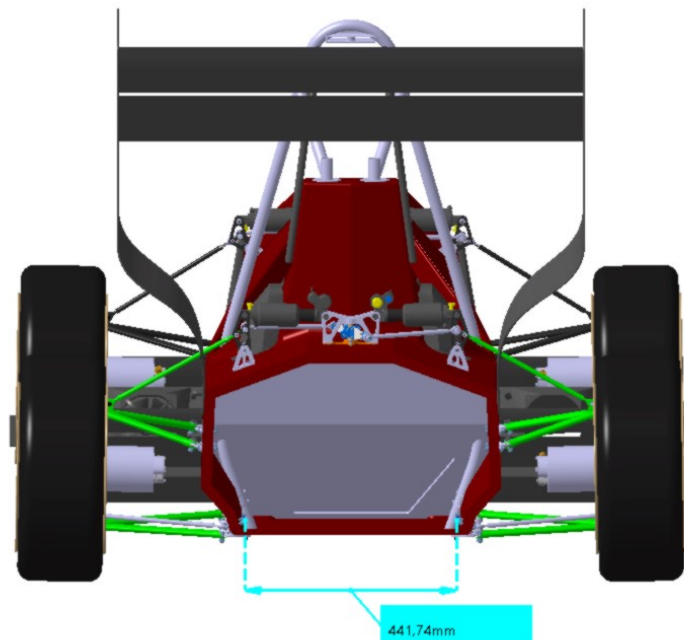
Figure 2.7: Suspension detail

The lower arms were longer than the upper arms to improve the camber recovery. The consequence was a reduced width in the lower part of the monocoque. Hence, considering the shrinkage and the space occupied by the bolts to fasten the arms to the monocoque, the remaining space was about 441 mm. The other two measures, the length and the height (respectively along x and z), were not subject to particular constraints. Obviously, both of them had to be as low as possible because an excessive length would have caused the motion of the centre of gravity of the battery pack towards the rear of the car, while an excessive height would have caused a higher centre of gravity. Moreover, all the components present in the rear compartment had to be considered such as the low voltage battery, the fuse box, the high voltage cables and so on. In conclusion, the battery pack was supposed to be as compact as possible in order to maintain the weight low.

## 2.6  Safety and reliability

The battery pack design is strongly influenced by the requirements in terms of safety. The constraints about this subject are stringent and they are well described in the rules [1]. The main rules for what concerns the safety from the structural point of view are reported below:

- *The TS accumulator container itself, the mounting of the TS accumulator container to the chassis and the mounting of the cells to the container must be designed to withstand the following accelerations:*

  - *40 g in the longitudinal direction (forward/aft)*
  - *40 g in the lateral direction (left/right)*
  - *20 g in the vertical direction (up/down)*

- *Any brackets used to mount the TS accumulator container must be made of steel 1,6 mm thick or aluminium 4 mm thick and must have gussets to carry bending loads. Each attachment point including brackets, backing plates and inserts, must be able to withstand 20 kN in any direction.*

The accelerations considered in the rules are typical of a crash. In case of an accident, the battery pack should be also well protected by the other elements belonging to the

car. The battery pack positioned in the rear compartment satisfies another requirement in terms of safety because it further increases the protection due to the presence of the main hoop which is in charge of guarding the driver in case of a rollover.

The safety requirements are not only structural but also electrical. When dealing with high voltage devices it is necessary to foresee insulation to eliminate the risk for the driver and for the people handling the objects considered. Moreover, the rules state that fire retardant materials must be used for the battery pack. Electrical safety must be then guaranteed by using fuse, AIRs, BMS and other printed circuit boards. They are used to keep under control current, voltage and temperature and to act in case of over-current, overvoltage, overtemperature or loss of insulation. The arrangement of these components was considered in the design stage in order to optimize the packaging.

Reliability is a very important aspect in a project. The performances without reliability are useless, therefore it must be considered in the design phase. The reliability of the project was ensured by adopting solutions like positive locking mechanisms. It also influenced the choice of different components of the battery pack because, in some situations, changing completely the solutions means to increase the risk in terms of reliability.

# Chapter 3

# Cell selection

## 3.1   Chemistry and geometry

Cell selection is one of the fundamental works in the design of a battery pack. There are different types of chemistry and geometry to choose from. The cells of interest for this application are the so called "secondary batteries". In this type of batteries, both the processes of charging and discharging can take place, i.e. the transformation of electrical energy into chemical energy and the reverse transformation from chemical to electrical [4].

The Lead-acid battery is the oldest technology. It is very popular due to its low cost and the low maintenance requirements. It has no memory effect, that is the loss of capacity due to the fact that the battery is repeatedly recharged after being only partially discharged [5]. Unfortunately, it presents some serious disadvantages which do not allow the usage for battery pack applications. They are the low energy density and the fact that it can only withstand a limited number of discharge cycles from fully charged to fully discharged. Moreover, the presence of lead does not make it an environmental friendly solution.

The Nickel-Cadmium (NiCd) battery is widely used, especially in applications where long life, low cost and high discharge rate are important. It can easily withstand rigorous working conditions without affecting the integrity of the cell. The energy density is slightly higher with respect to the Lead-acid solution but unfortunately it presents memory effect and the metals used are highly toxic.

An alternative to the NiCd technology is the Nickel-Metal Hydride (NiMH) battery.

It solves the problem of toxic materials, shows a higher energy density and reduces the memory effect. These advantages are counteracted by a lower cycle life especially in case of demanding working conditions and by a higher cost.

The Lithium-ion (Li-ion) battery represents the best technology at the moment available on the market. It ensures a considerably higher energy density with respect to the other solutions providing an excellent solution in applications in which the weight is a primary goal. Moreover, it does not present the memory effect. The cost is higher than the other solutions and it requires a protection circuit in order not to ruin its performances. *Figure 3.1* shows the comparison between the main Li-ion technologies.
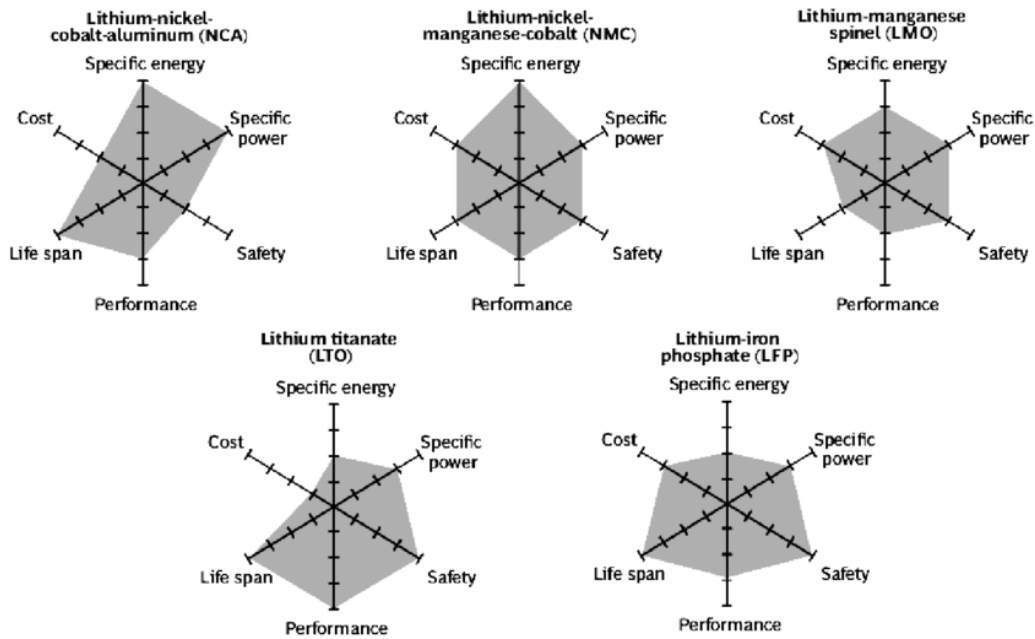


Figure 3.1: Li-ion comparison [6]

An alternative to Li-ion battery is represented by the Lithium-polymer (Li-po). The only difference between them is identified by the electrolyte separating the anode and the cathode. In Li-ion it is liquid while in Li-po can be a dry solid, a porous chemical compound or a gel [4].

Besides the different chemistry, there are also different geometries to consider. The most typical shape is the cylindrical one (*figure 3.2a*). It guarantees good mechanical

(a) Cylindrical          (b) Prismatic          (c) Pouch

Figure 3.2: Cell Shapes

stability and low cost being easy to manufacture. The cylindrical shape does not offer high efficiency from a space utilization point of view leaving air cavities between cells. This aspect is counteracted by its high energy density and by the fact that the space between cells can be used for cooling purposes. Then it can be equipped with safety features, shown in *figure 3.3* not present in other geometries.
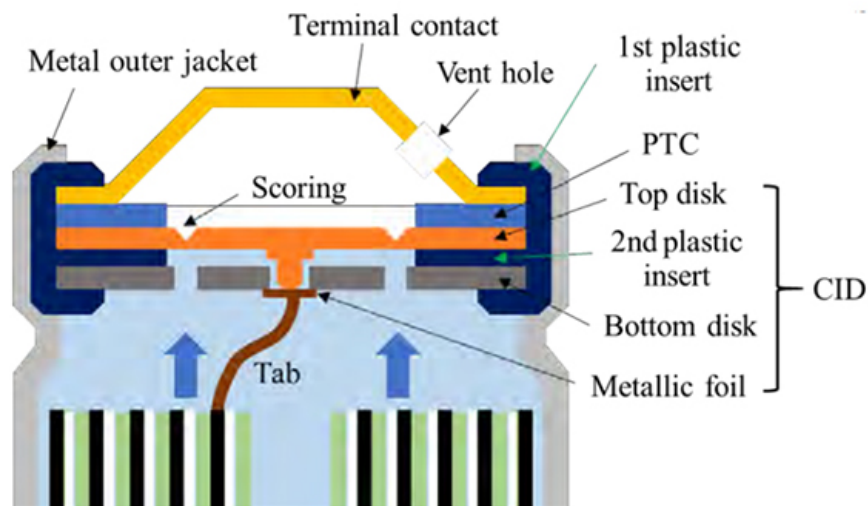


Figure 3.3: Safety devices in a cylindrical cell [7]

The first safety device is the current interrupt device (CID), which disconnect permanently the electrical circuit in case of excessive pressure, by braking the top disk. The positive thermal coefficient (PTC) is a device in which the resistance is proportional

23

to the temperature, so that in case of overtemperature the resistance increases reducing the current passage. The PTC is reversible at the contrary of the CID, in fact the resistance decreases when the temperature returns to acceptable levels, restoring the initial characteristics of the cell. The last safety device is the vent hole which allows the escaping of gas thus avoiding internal pressure increase.

The prismatic cells (*figure 3.2b*) have a cover made of aluminium or steel to ensure mechanical stability. They provide a better utilization of the space in comparison with the cylindrical ones. Although, they suffer of swelling, that is an expansion due to the gas formation inside the cell, so additional space must be considered in the design stage. Moreover they typically have a shorter life with respect to the cylindrical cells.

The pouch geometry (*figure 3.2c*) is typically of the Li-po chemistry. The main difference is represented by the external cover made of an aluminium-plastic composite film which is flexible. The absence of a rigid case makes this solution light. The space utilization is more efficient but the swelling problem is even more emphasized. Also in this case, in the design stage some space must be left free for swelling, anyway a certain stack pressure must be provided. Moreover, the low profile does not allow the usage of the safety devices present in the cylindrical configuration.

In 2017 the car was equipped with Li-po prismatic cells. This type of batteries were used by the majority of the teams competing in Formula SAE. In 2018 the team decided to adopt the Li-ion cylindrical cells. The comparison between the cylindrical Li-ion Sony VTC6 used in 2018 and a possible prismatic Li-po solution is shown in *table 3.1* . By considering two similar pack configurations, as far as energy concerns, it was evident the difference in batteries' weight. Thanks to the higher energy density of the Li-ion cylindrical cell, the two solutions differ from each other by 9,35 kg, which means significantly higher performances of the car. The price to pay for the high energy density was an increased complexity in terms of temperature management. The Li-po cell shows a greater current rating, index of the fact that the cell is less affected from a thermal point of view, indeed, the teams adopting this solution in many cases do not even use any cooling system. Despite this drawback, the Sony VTC6 was the chosen cell because the thermal performance was not so low to force the introduction of a liquid cooling system [8]. This change of technology introduced in 2018 put the basis to reduce the gap in terms of weight with the top teams.

|                                            | **Sony VTC6** | **Melasta LPA542126** |
|--------------------------------------------|:-------------:|:---------------------:|
| Chemistry                                  | Li-ion        | Li-po                 |
| Nominal capacity [mAh]                     | 3120          | 6000                  |
| Nominal Voltage [V]                        | 3,6           | 3,7                   |
| Weight [g]                                 | 46,8          | 127,0                 |
| Energy density [Wh/g]                      | 0,240         | 0,175                 |
| Maximum continuous discharge current [A]   | 20            | 56                    |
| Pack configuration                         | 4p-140s       | 2p-140s               |
| Pack nominal energy [kWh]                  | 6,289         | 6,219                 |
| Pack weight (only cells) [kg]              | 26,21         | 35,56                 |
| Maximum continuous discharge current [A]   | 80            | 112                   |

Table 3.1: Comparison between 2018's cell and a possible prismatic cell

## 3.2 Possible configurations

Once the type of chemistry and geometry was chosen, different solution were taken into account. The *table 3.2* summarizes the batteries taken into account and their characteristics. The batteries diameter and length are expressed by a code of five digits (e.g. 18650). The first two digits represents the cell's diameter in millimetres while the third and fourth digits stand for the length in millimetres. So, the 18650 batteries have a diameter of 18 mm and a length of 65 mm while the 21700 batteries have a diameter of 21 mm and a length of 70 mm.

The Sony VTC6 was the cell used in 2018, while the LG HG2 and the Samsung 30Q were competitors' batteries having the same chemistry and dimensions. They were similar in every aspect, but at the first look the VTC6 seemed better than the other two. It had the highest capacity and the highest current rating among the 18650 and an energy density equal to the 30Q. However, the data from datasheets are not

| | Sony VTC6 | Lg HG2 | Samsung 30Q | Samsung 30T | Samsung 40T |
|---|---|---|---|---|---|
| Dimensions | 18650 | 18650 | 18650 | 21700 | 21700 |
| Nominal capacity [mAh] | 3120 | 3000 | 3040 | 3000 | 4000 |
| Nominal voltage [V] | 3,6 | 3,6 | 3,6 | 3,6 | 3,6 |
| Weight [kg] | 46,8 | 47,0 | 45,6 | 68,3 | 66,6 |
| Energy density [Wh/g] | 0,240 | 0,230 | 0,240 | 0,158 | 0,216 |
| Internal impedance [Ω] | 0,13 | 0,20 | 0,13 | 0,13 | 0,12 |
| Maximum continuous discharge current [A] | 20 | 20 | 15 | 35 | 35 |

Table 3.2: Possible cells for 2019's battery pack

always correct and they tend to be optimistic. For this reason some tests were carried out on these three to understand which one was the best among the 18650 batteries. The tests were already performed in the season 2017/18 and presented by Maglio in 2019 [8].

The cycle in *figure 3.4* represents the power profile used for the test. It was extrapolated by the data collected during 2017's races, by taking the battery pack power and then appropriately scaling it on a single cell by dividing for the total number of cells present into the configuration considered (720 cells). The power RMS of this cycle was equal to 27 W on a single cell, which multiplied by the total number of cells was equal to 19,4 kW of RMS. The test was considered finished when the temperature reached the threshold temperature equal to 60°C, that was the limit imposed by competition's rules. *Figure 3.5* shows the temperature trends of the three cells. The Sony VTC6 performed better than the others, reaching the temperature limit much later. From the voltage detail in *figure 3.6* is possible to see the differences among the cells for what concerns the voltage drop. The VTC6 experienced a smaller drop, index of the lower internal resistance. This characteristic was the main factor which allowed the cell to perform better. *Figure 3.7* and *figure 3.8* represent the voltage and the current trends respectively. The following analysis allowed to choose among the 18650 batteries, for this reason the 30Q and the HG2 were no longer considered among the possible solutions.
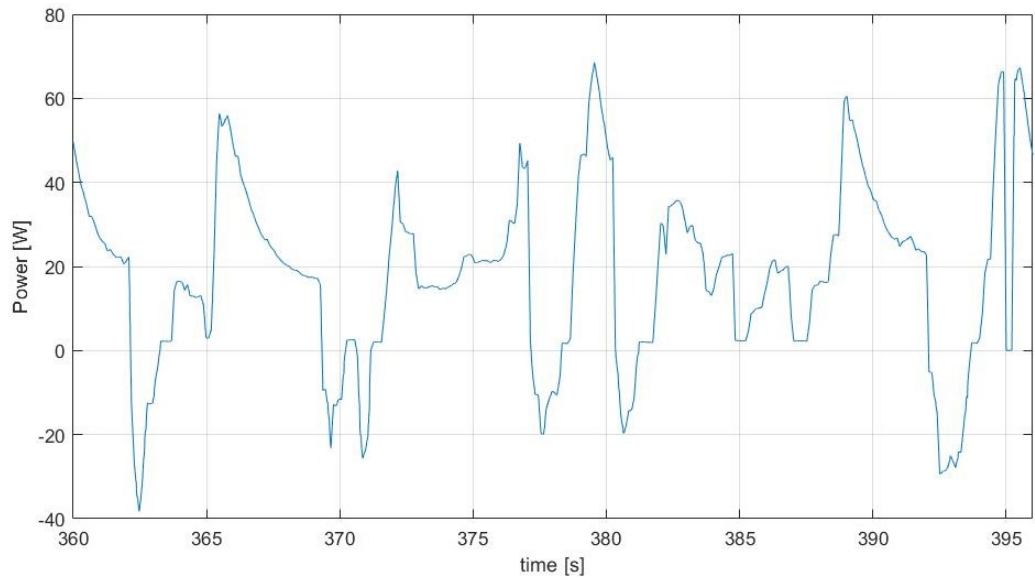
Figure 3.4: Test on 18650 batteries: power cycle
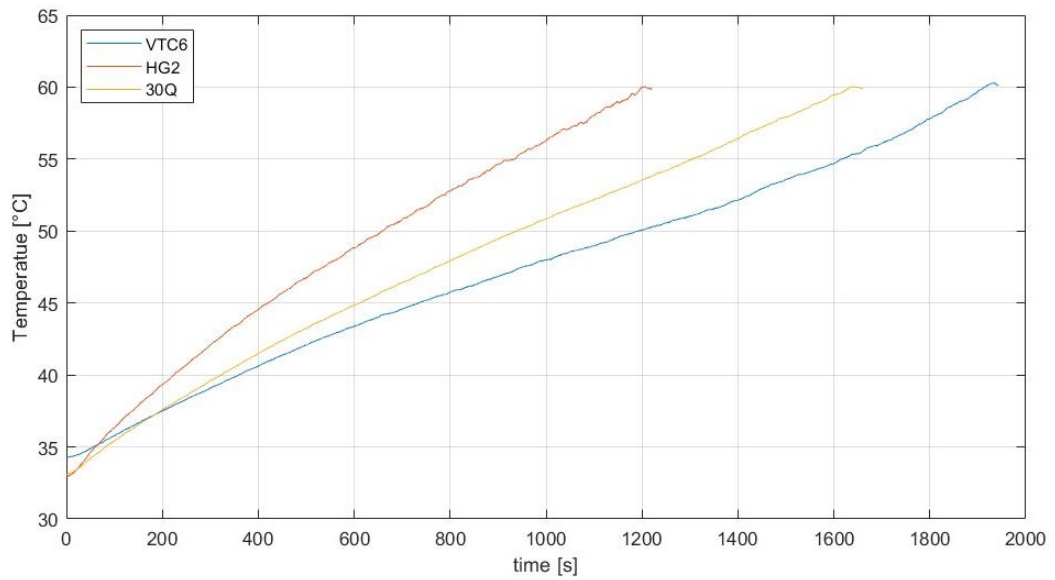


Figure 3.5: Test on 18650 batteries: temperature comparison
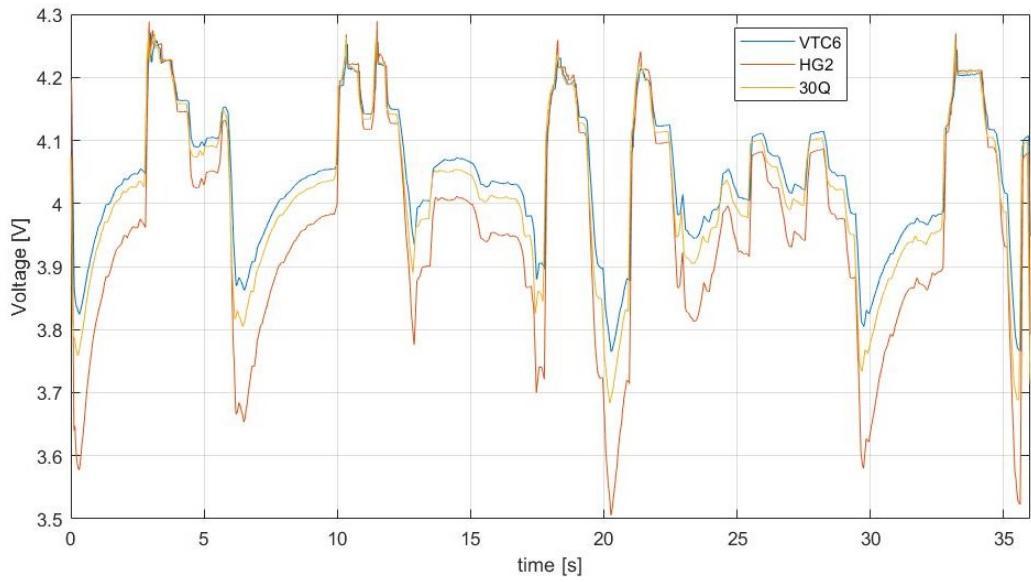
Figure 3.6: Test on 18650 batteries: voltage drop comparison
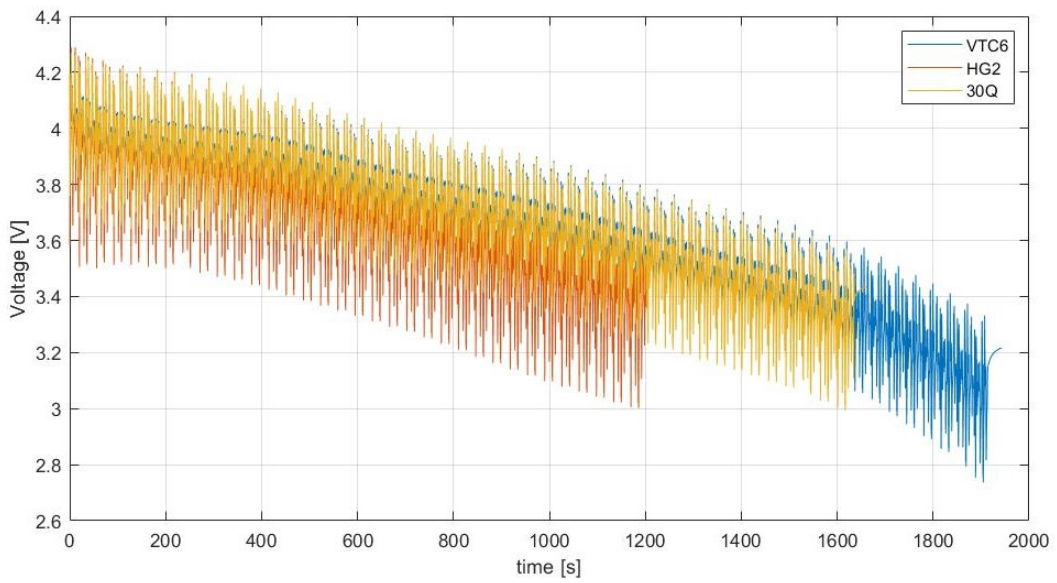


Figure 3.7: Test on 18650 batteries: voltage comparison

28
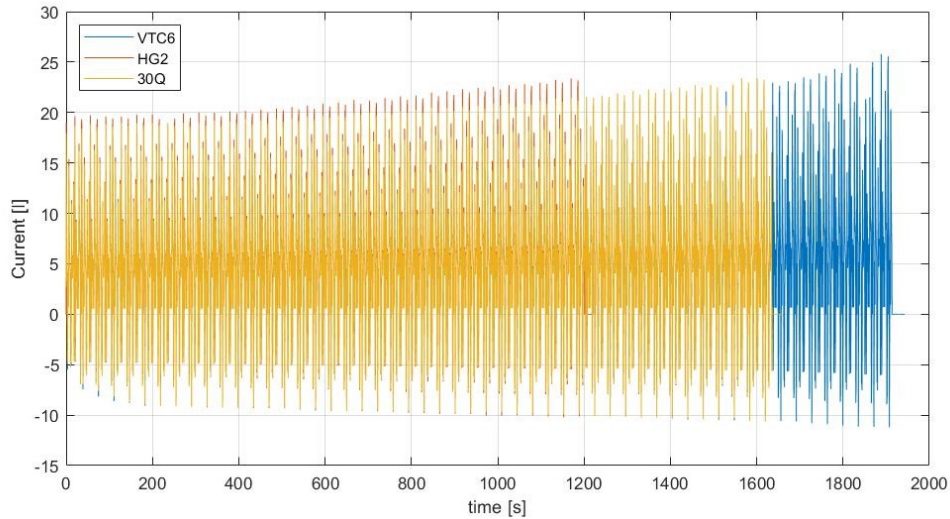
Figure 3.8: Test on 18650 batteries: current comparison

Once the 18650 was chosen, the second step was about comparing it with the remaining 21700 cells. This time it was not possible to make a direct comparison because the cells were very different from each other. Hence, each cell was considered with its possible battery pack configuration. The following solutions were taken into account:

- **Solution 1**: 720 cells Sony VTC6 with configuration 5p-144s divided in 6 modules connected in series.

- **Solution 2**: 576 cells Sony VTC6 with configuration 4p-144s divided in 6 modules connected in series.

- **Solution 3**: 560 cells Sony VTC6 with configuration 4p-140s divided in 5 modules connected in series.

- **Solution 4**: 560 cells Sony VTC6 with configuration 4p-140s divided in 5 modules connected in series.

- **Solution 5**: 420 cells Sony VTC6 with configuration 3p-140s divided in 5 modules connected in series.

- **Solution 6**: 420 cells Sony VTC6 with configuration 3p-140s divided in 5 modules connected in series.

| | VTC6 | | | 30T | | 40T |
|---|---|---|---|---|---|---|
| | **1** | **2** | **3** | **4** | **5** | **6** |
| ✕ Configuration | 6 X 5p24s | 6 X 4p24s | 5 X 4p28s | 5 X 4p28s | 5 X 3p28s | 5 X 3p28s |
| ⚡ Maximum voltage | 600 V | 600 V | 588 V | 588 V | 588 V | 588 V |
| 🔋 Nominal energy | 8,09 kWh | 6,47 kWh | 6,29 kWh | 6,05 kWh | 4,54 kWh | 6,05 kWh |
| ⚖ Weight | 33,70 kg | 26,96 kg | 26,21 kg | 38,25 kg | 28,69 kg | 27,97 kg |
| 📐 Dimensions | x=715 mm y=441 mm z=179 mm | x=715 mm y=441 mm z=155 mm | x=791 mm y=368 mm z=155 mm | x=875 mm y=393 mm z=167 mm | x=875 mm y=393 mm z=140 mm | x=875 mm y=393 mm z=140 mm |

✕ Configuration ⚡ Maximum voltage 🔋 Nominal energy ⚖ Weight 📐 Dimensions

Figure 3.9: Possible configurations

The characteristics of each configuration are summarized in *figure 3.9*. The solutions were selected taking into account the constraints and the targets explained in the previous chapter. The weight indicated was not an estimation of the total pack weight but only the total mass of the cells. The dimensions were estimated considering the same module and pack configurations, shown in *figure 3.10*, for all the six solutions.
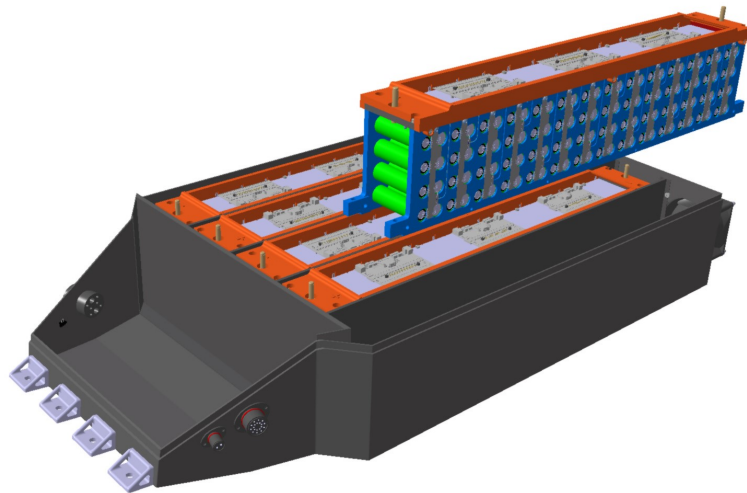


Figure 3.10: Considered module configuration
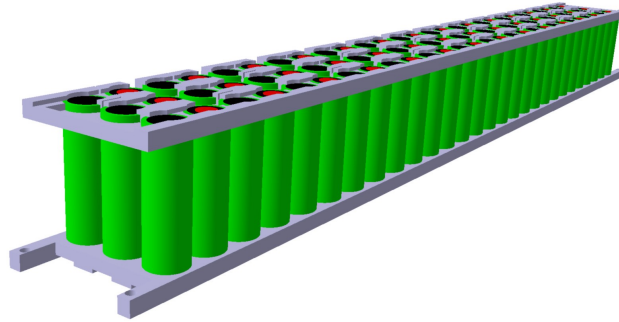
Figure 3.11: Alternative module configuration

A different module configuration was also taken into account with cells arranged in a vertical position with respect to the ground as in *figure 3.11*. It was not considered of interest because it did not add any particular advantage in terms of packaging or cooling. On the contrary, it would have added complexity in terms of electrical connections and thermistors positioning because in cylindrical cells the two poles of the cells are located opposite to each other, so one end would have been positioned in proximity of the container floor. Usually the vertical positioning of the cells is successful in case of prismatic cells in which the two poles are located on the same side.

## 3.3   Cells test

To have an idea of the thermal behaviour of the 3 cells, a simple test was developed. It was not possible to repeat the same test done for the 18650 cells because the equipment was not available in that particular period. For this reason the experiment was performed connecting the tested cell to a simple battery analyser, and by registering the temperatures using a thermistor and a thermal camera (*figure 3.12*).

The test was a simple duty cycle 6 seconds long: 4 seconds in which power was requested and 2 seconds in which power was not requested. The power profile was typical of a long straight followed by a curve. The power was derived from the total pack power and then scaled on the single cell. The cycle was then repeated until the cell was fully discharged. The test conditions were therefore the following:
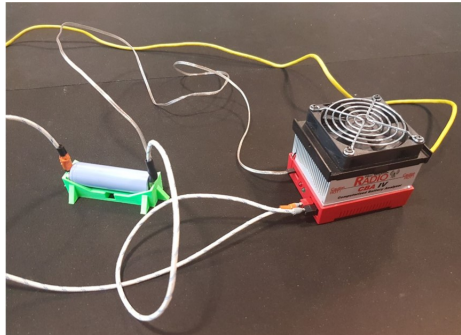
(a) Battery analyser
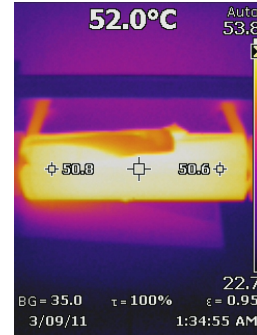


(b) Thermal camera

Figure 3.12: Test instruments

- Duty cycle (values related to battery pack)

    - 40 kW for 4 s

    - 0 kW for 2 s

    - Power RMS = 26,7 kW

- No charging power

- Repeated till full discharge

The RMS of this test (26,7 kW) was set considerably higher than the RMS characterizing the test on 18650 (19,4 kW). In this case the experiment was not representative of a real race but was a sort of stress test to monitor the cells reaction to high discharge conditions. Moreover, the simple equipment was not able to give current to the cell, but only to draw current from it, therefore the regenerative braking was not simulated. Even if particular attention was used to electrical connect the cells to the battery analyser, surely the resistance was higher with respect to a specific testing machine for batteries. This additional factor added to what already said makes this test valuable only for a direct comparison among cells.

In *table 3.3* are reported all test conditions and results. In *figure 3.13* are instead shown the voltage versus capacity graphs related to each cell discharge.

| | | Solution | 1 | 2 | 3 | 4 | 5 | 6 |
|---|---|---|---|---|---|---|---|---|
| **Cell characteristics** | | **Name** | VTC6 | VTC6 | VTC6 | 30T | 30T | 40T |
| | | **Rated Capacity [Ah]** | 3,12 | 3,12 | 3,12 | 3,00 | 3,00 | 4,00 |
| | | **Rated Energy [Wh]** | 11,232 | 11,232 | 11,232 | 10,800 | 10,800 | 14,400 |
| **Pack characteristics** | | **Module configuration** | 5p 24s | 4p 24s | 4p 28s | 4p 28s | 3p 28s | 3p 28s |
| | | **Number of Modules** | 6 | 6 | 5 | 5 | 5 | 5 |
| | | **Number of Cells** | 720 | 576 | 560 | 560 | 420 | 420 |
| **Duty cycle characteristics** | | **Power ON [W]** | 55,6 | 69,4 | 71,4 | 71,4 | 95,2 | 95,2 |
| | | **Time ON [s]** | 4 | 4 | 4 | 4 | 4 | 4 |
| | | **Power OFF [W]** | 0 | 0 | 0 | 0 | 0 | 0 |
| | | **Time OFF [s]** | 2 | 2 | 2 | 2 | 2 | 2 |
| **Initial conditions** | | **Starting Voltage [V]** | 4,203 | 4,202 | 4,201 | 4,202 | 4,203 | 4,203 |
| | | **T initial [°C]** | 26,8 | 27,1 | 26,6 | 27,0 | 26,4 | 27,8 |
| **Results** | | **Discharge Time [mm:ss]** | 16:04 | 12:35 | 12:11 | 13:22 | 09:58 | 11:41 |
| | | **Capacity Used [Ah]** | 2,948 | 2,918 | 2,898 | 3,078 | 3,106 | 3,694 |
| | | **Capacity Used [%]** | 94,5% | 93,5% | 92,9% | 102,6% | 103,5% | 92,4% |
| | | **Energy Used [Wh]** | 9,848 | 9,599 | 9,364 | 10,607 | 10,358 | 12,184 |
| | | **Energy Used [%]** | 91,2% | 88,9% | 86,7% | 98,2% | 95,9% | 84,6% |
| | | **T final [°C]** | 49,0 | 57,9 | 61,3 | 37,0 | 49,7 | 60,5 |
| | | **ΔT [°C]** | 22,2 | 30,8 | 34,7 | 10,0 | 23,3 | 32,7 |

Table 3.3: Cells test resume
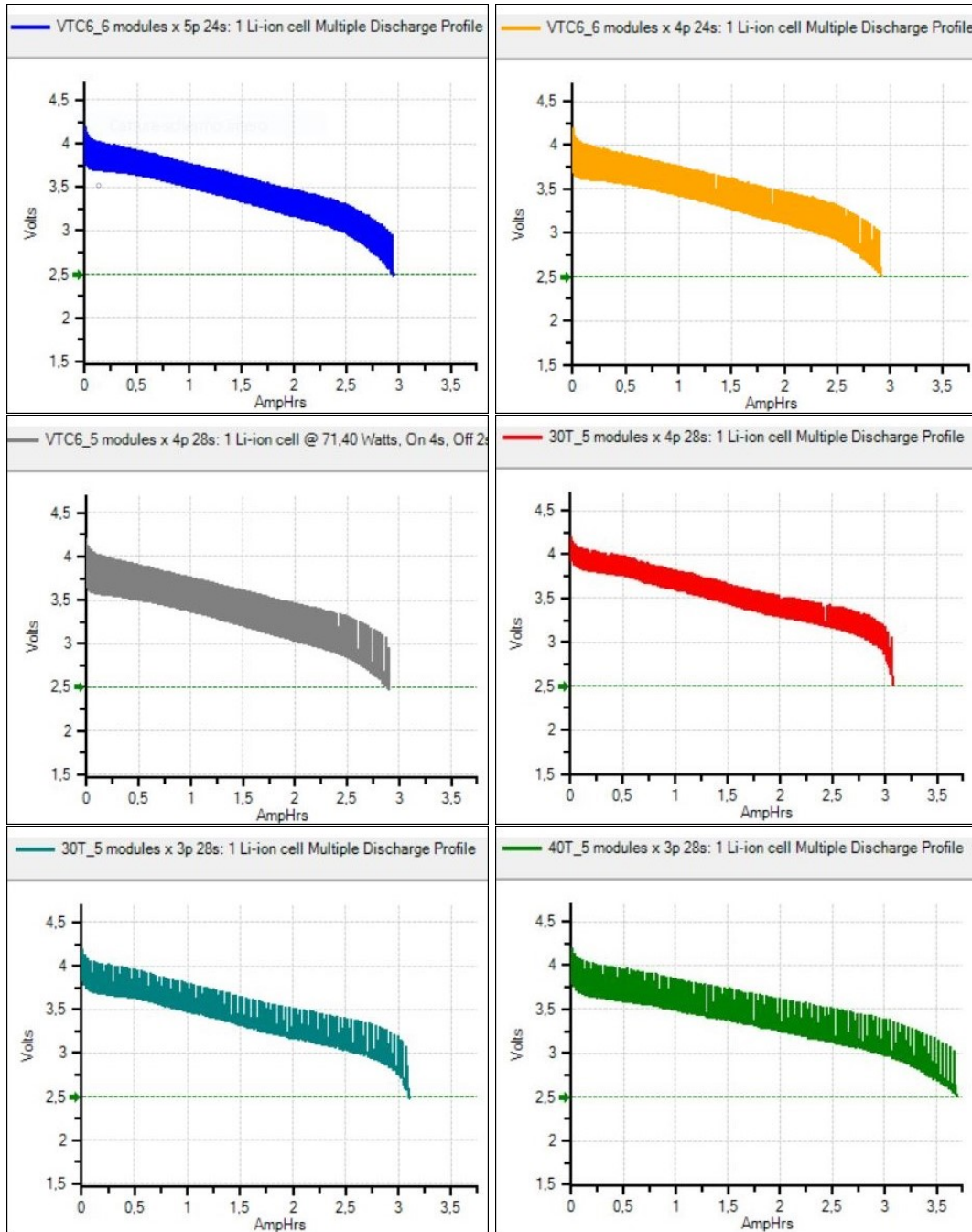
Figure 3.13: Cells test results: Voltage vs Capacity

| | X-dimension | Y-dimension | Z-dimension | Volume | Weight | Energy | Temperature | Efficiency | Score |
|---|---|---|---|---|---|---|---|---|---|
| Solution 1 | 10,0 | 0,0 | 0,0 | 0,8 | 3,8 | 0,0 | 5,1 | 4,9 | 24,5 |
| Solution 2 | 10,0 | 0,0 | 6,2 | 7,0 | 9,4 | 7,9 | 1,6 | 3,2 | 45,1 |
| Solution 3 | 5,3 | 10,0 | 6,2 | 10,0 | 10,0 | 8,7 | 0,0 | 1,5 | 51,7 |
| Solution 4 | 0,0 | 6,6 | 3,1 | 0,0 | 0,0 | 9,9 | 10,0 | 10,0 | 39,6 |
| Solution 5 | 0,0 | 6,6 | 10,0 | 7,6 | 7,9 | -7,2 | 4,6 | 8,3 | 37,8 |
| Solution 6 | 0,0 | 6,6 | 10,0 | 7,6 | 8,5 | 9,9 | 0,8 | 0,0 | 43,4 |

Table 3.4: Score of the different solutions

## 3.4 Final choice

The overview of the characteristics of each solution proposed is presented in *figure 3.14*, together with the results obtained in the test described in the previous section.

To each solution was then assigned a score computed as the sum of the individual scores regarding each specific characteristic. The score related to the single characteristic was evaluated in a relative way, considering the best and worst values as a reference and assigning to them 10 and 0 respectively. All the scores are reported in *table 3.4*.

The rule was modified for the score assigned to the energy, for which instead was used the target value 6,03 kWh (value obtained and explained in the previous chapter) as reference for the highest score. It was then given a relative score considering the worst value as reference for the lowest score. Besides, the score was positive in the case in which the energy was higher than the reference, but it was negative in case of value lower than the threshold. This explains the negative score given to the energy of solution 5.

The following considerations were done:

- **Solution 1** (VTC6, 6 modules x 5p-24s): it was the solution adopted in 2018 when the regenerative braking was not correctly implemented. It was characterized by a surplus of energy and a consequent excess of weight.

- **Solution 2** (VTC6, 6 modules x 4p-24s): this solution was good for what concerns energy and weight. It had one parallel connection less with respect to the solution 1, that inevitably would have increased the current and consequently the temperature. This was a disadvantage considered manageable with the cooling system. The 6 modules configuration favoured the dimension limitation in
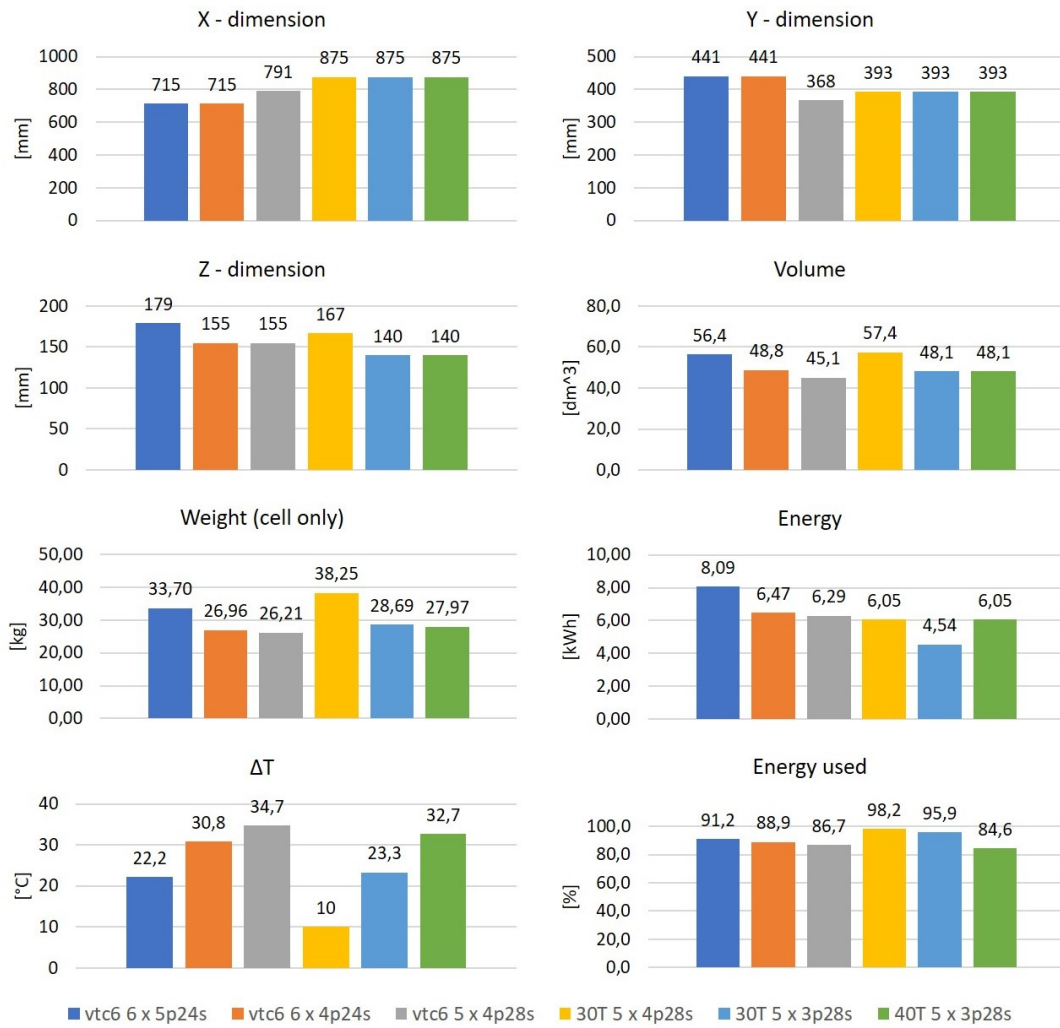
Figure 3.14: Characteristics comparison

longitudinal direction rather than in transversal direction. As explained in the previous chapter, the longitudinal direction was not subjected to severe limitations while the transversal direction was more important. This configuration, even if suitable, would have not allowed the introduction of the lateral cooling ducts.

- **Solution 3** (VTC6, 5 modules x 4p-28s): this was the selected configuration. It was the best in terms of volume and weight. The major drawback was represented by the thermal behaviour, which however was considered manageable, also because the 5 modules configuration allowed the introduction of new cooling features: bigger fans and lateral cooling ducts.

- **Solution 4** (30T, 5 modules x 4p-28s): it was the best from the thermal point of view, but the weight and the volume were too high.

- **Solution 5** (30T, 5 modules x 3p-28s): the major drawback was represented by the energy, probably insufficient also in case of aggressive regenerative braking.

- **Solution 6** (40T, 5 modules x 3p-28s): Even if the energy, weight and volume were good, the cell did not show a good thermal behaviour.

The Sony VTC6 was therefore confirmed as the final choice, but with a battery pack configuration different from the one of the 2018. The other cells did not present enough advantages to justify a change, that would have added work in terms of development of cell model and uncertainty for the use of a new battery.

# Chapter 4

# Thermal optimization

## 4.1 Overview of cooling systems

In automotive applications there is the need for battery cooling systems, especially in the case in which the current profile requested is demanding as in race cars. The power dissipated by heat is obtained through the following formula:

$$P = R I^2 \tag{4.1}$$

The higher are the current ($I$) and the resistance ($R$), the higher is the power dissipated by heat ($P$).

The main means used for battery pack cooling purposes are:

- air,

- liquid,

- phase change material (PCM).

The air cooling system is the less complicated way to cool down the batteries. The air passes through the cavities among cells and carries away the heat generated. This system is not the most effective if the goal of the cooling system is to reduce the battery pack temperature or to maintain the temperature constant at a certain level. When the air flows through the cells, it gradually increases its temperature causing the uneven temperature distribution typical of the air cooling systems. Cells which

have different temperatures, discharge in different ways because the efficiency of the batteries is temperature dependent. This can cause, after a high number of cycles, some batteries to be more ruined than the others. Despite these disadvantages, it is still an attractive solution for applications in which the lightweight is the main goal. It does not need pipes or radiators, hence the weight added with this cooling system is very low.

The liquid cooling system is the most effective way to manage the temperature inside a battery pack. The liquid (water or coolant) has better thermodynamics properties than the air, indeed the heat capacity and the heat conductivity are higher. For this reason, it is the most used system in passengers electric vehicles. The main drawbacks are the higher complexity (with respect to air cooling), the weight and the risk of leaking. All these factors are due to the recirculating pipes filled with fluid running through the car. Moreover, there is the a need for a heat exchanger.

The liquid cooling system can be indirect or direct. The direct one is similar to the cooling system used in vehicles equipped with internal combustion engines, in which the coolant flows inside pipes located close to the cells. In an indirect cooling system, the cooling medium is a liquid that directly flows through the cells. The liquid in this case is a dielectric fluid non-conductive. This last technology is still in the first stages of development.

The last option is the usage of phase change materials (PCM) shown in *figure 4.1*.
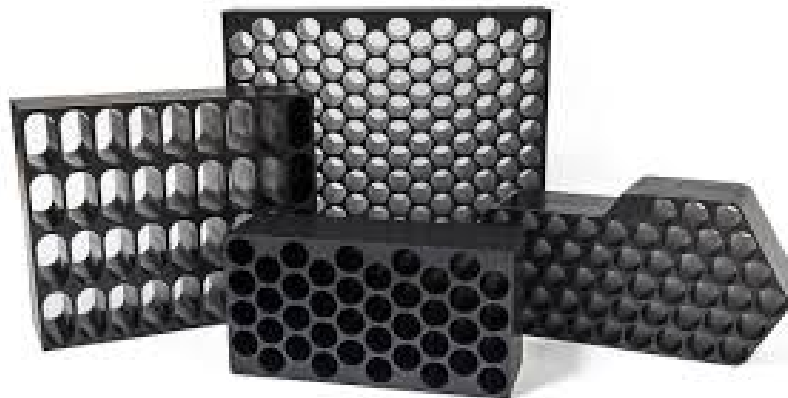


Figure 4.1: PCM cooling

When the temperature increases inside the module, the PCM starts the phase change from solid to liquid. During the state passage, the material absorbs significant amount of heat by only experiencing few degrees of temperature increase. This property is used to maintain the temperature under control in battery packs. The PCM is only able to store the heat so it cannot carry away the heat collected. This type of technology is therefore considered passive. In order to be used inside battery packs for vehicles, it has to be combined with an active cooling system.

The choice for the SC19 battery pack fell on an air cooling system with the concept illustrated in *figure 4.2*, a solution that was confirmed from the previous year. The air entered from the a cut obtained in the top cover (blue shape) and came out from the rear part of the battery pack in correspondence of the fans (red).

It was considered a sufficient solution for this application in which the battery life was not important since the kilometres run by the car was limited. In a case in which the battery life was considered of interest, a liquid cooling system should be the preferable choice to maintain the temperature in the range of maximum cells efficiency, without stressing them too much. The liquid cooling system with all its extra equipment (pipes and heat exchanger) would have been too heavy.

By maintaining the same solution adopted the previous year, it was possible to execute some tests directly on the SC18 battery pack and cooling system. They are explained in the next chapters.
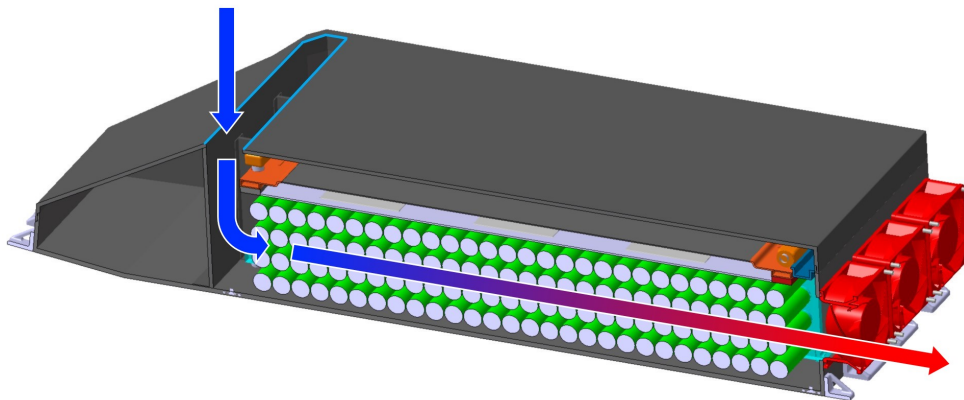


Figure 4.2: Air cooling system

## 4.2 Intake manifold

The first test carried out was aimed at evaluating the effectiveness of the system used to introduce air inside the modules of the battery pack. It was a track test in which the car was driven for 22 km to simulate the endurance event. It was repeated two times in the same day to have the environmental conditions as constant as possible. Also the pilot was not substituted to maintain the same driving behaviour and therefore a similar power profile. The only difference between the two simulations was represented by the intake system used for cooling down the battery pack.

In the 2018's configuration, the air entering into the modules was drawn from the rear compartment of the car (*figure 4.3a*). There were two holes obtained in the monocoque to allow the recirculation of air.

The second configuration (*figure 4.3b*) featured an intake manifold to directly take the air from the external environment. The two intakes of the manifold were placed in the holes that previously were used as air recirculating holes.

The temperature in the two simulations was around 16°C. It was not representative of an endurance run in the summer where the environmental temperature could also reach 35°C, but it was not of particular interest since the main objective was the difference between the two configurations in equal conditions.



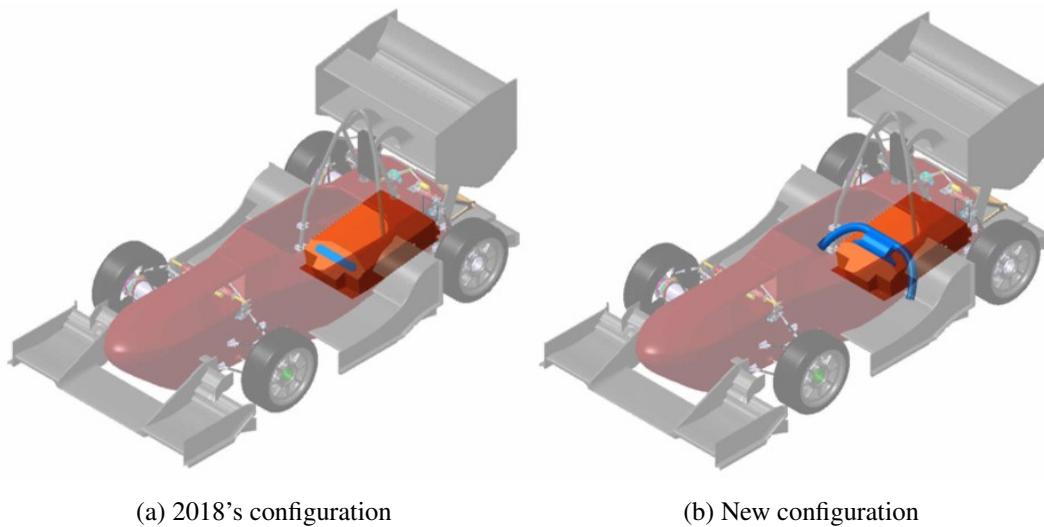(a) 2018's configuration           (b) New configuration

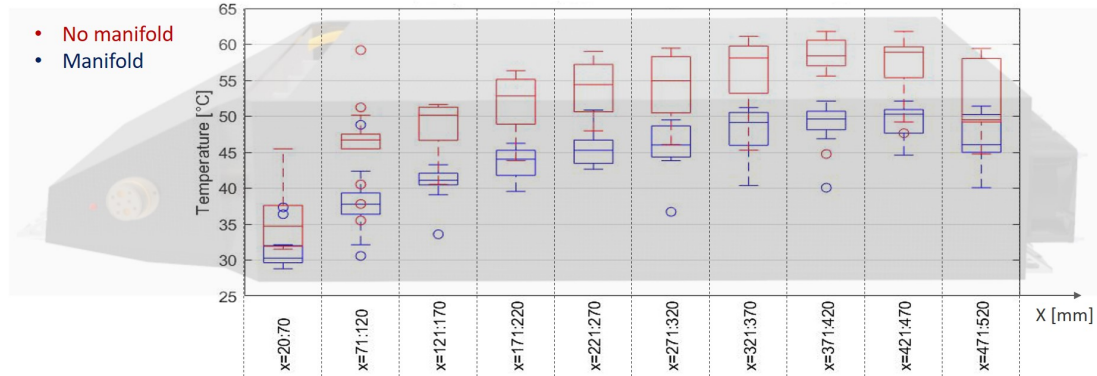Figure 4.3: Manifold configurations used during track test

Figure 4.4: Intake manifold test results

All the temperatures coming from the NTC thermistors present on the battery pack to control the temperature were collected. The test results are shown in *figure 4.4*. The graph represents the temperature of the thermistors at the end of the two tests, with (blue) and without (red) intake manifold. The thermistors are grouped according to their distance X from the front vertical wall. The temperature distribution of each group is represented by a box plot to facilitate the comparison between different groups. The mean temperature going towards the end of the battery pack increases because along the path the air becomes gradually hotter due to the heat exchange.

The difference between the two configurations was noteworthy. The temperatures obtained using the intake manifold were clearly lower than the temperatures without duct. The mean values of the temperatures with the intake manifold were on average 7,6°C lower. Some of the outliers present were caused by some damaged thermistors as well as the temperature reduction in the last section of the battery pack. Despite these imperfections the test was successful because the error was constant in the two tests, hence irrelevant in the comparison of the two solutions. The problem of the 2018's solution was the air collected in the rear compartment. It was not fresh, but it was affected by the heat generated from other sources like the low voltage battery, the CPU and the electronic components.

The introduction of the intake manifold resulted beneficial and was therefore adopted for the 2019. The only difference with respect to the solution tested was that the intake manifold inlets were placed in a different position. They were no more put in the lower part of the car behind the sidepods because in that position lot of dust entered

the manifold. The solution was to place them in the higher part of the car, just above the pilot's shoulders, a zone of high pressure far from the dust of the asphalt (*figure 4.5*). The shape of the manifold was modelled according to the obstructions present in the rear compartment.
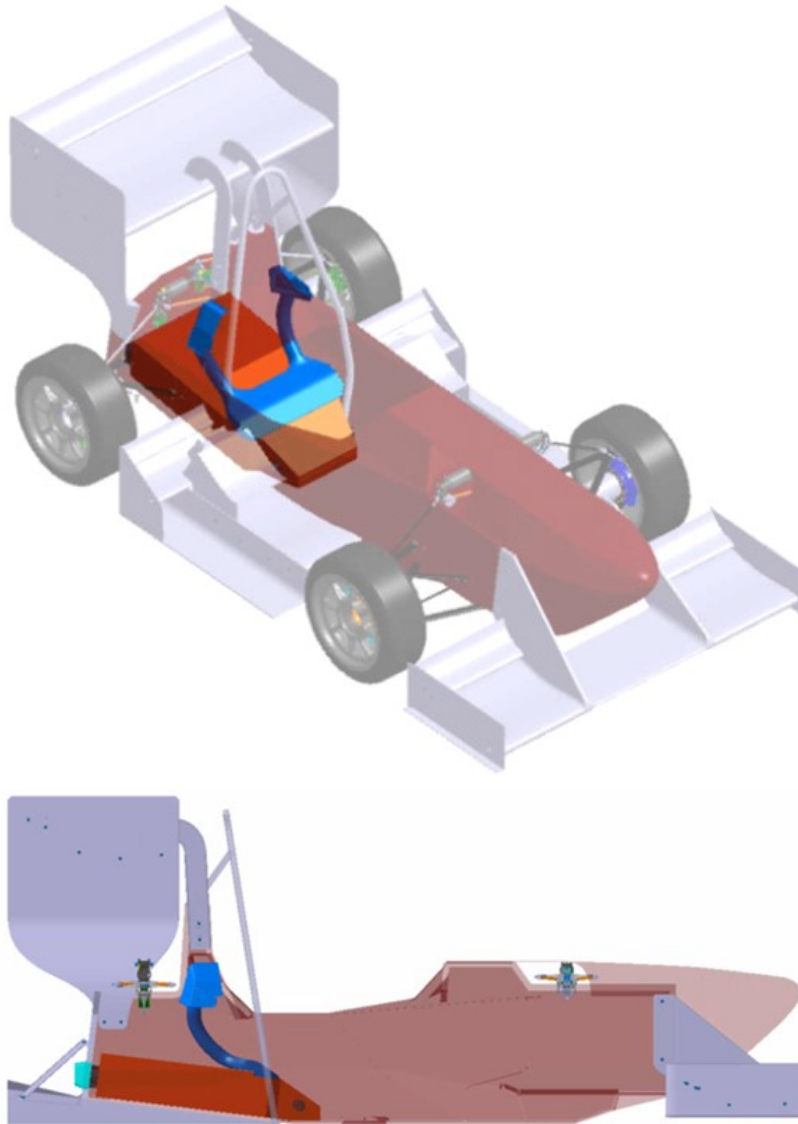


Figure 4.5: 2019's intake manifold

## 4.3 Regenerative braking

One of the main problems in the 2018's races was the regenerative braking. There was no deep knowledge of this aspect which resulted in wrong choices during the races. The problem was not related to the energy, that resulted sufficient because of the over dimensioning, but to the temperature of the battery pack. In the races, there was the worry about overheating due to the high external temperature of the environment. The solution to this problem was to run without using the regenerative braking, avoiding the current entering the battery pack during deceleration. The idea behind this choice was to reduce the thermal stress on the cells at least during braking.

The following test was performed to understand the thermal response of the cells with and without regenerative current. It was executed in a thermal chamber to keep the surrounding temperature under control (*figure 4.6*). It was not used the whole 2018's battery pack but only one module because of the dimensions of the testing machine. The single module was put inside a 3D printed container equipped with an intake hole and a fan to simulate the environment of the battery pack.



Figure 4.6: Thermal chamber for testing

The discharge power profile of both tests was derived from the 2018 Spain's race. For the second test it was added also the charging power. To obtain a reasonable charging profile the signal of the brake pedal sensor was used as reference. The regenerative power was set proportional to the pedal travel and was scaled to obtain a plausible percentage of regenerated energy. In this case the regenerated energy was equal to 26,8% of the total energy, which was acceptable and below the average recoverable percentage equal to 33%. The temperature in the chamber was set at 25°C.

The two power profiles and the correspondent thermal behaviours are shown in *figure 4.7*. Each line in the temperature versus time graph represents one thermistor of the module. The outcome of the test underlined that the usage of regenerative power did not increase the temperatures but, on the contrary, it decreased them in a significant way. The difference between the maximum temperatures of the two tests was equal to 8,3°C. The regenerative power allowed to maintain a higher SOC, which resulted in a higher voltage and therefore, with the same power, in lower current. This result showed that the choice of avoiding the regenerative braking during the race was a mistake but, on the contrary, it would have resulted beneficial from the thermal point of view.
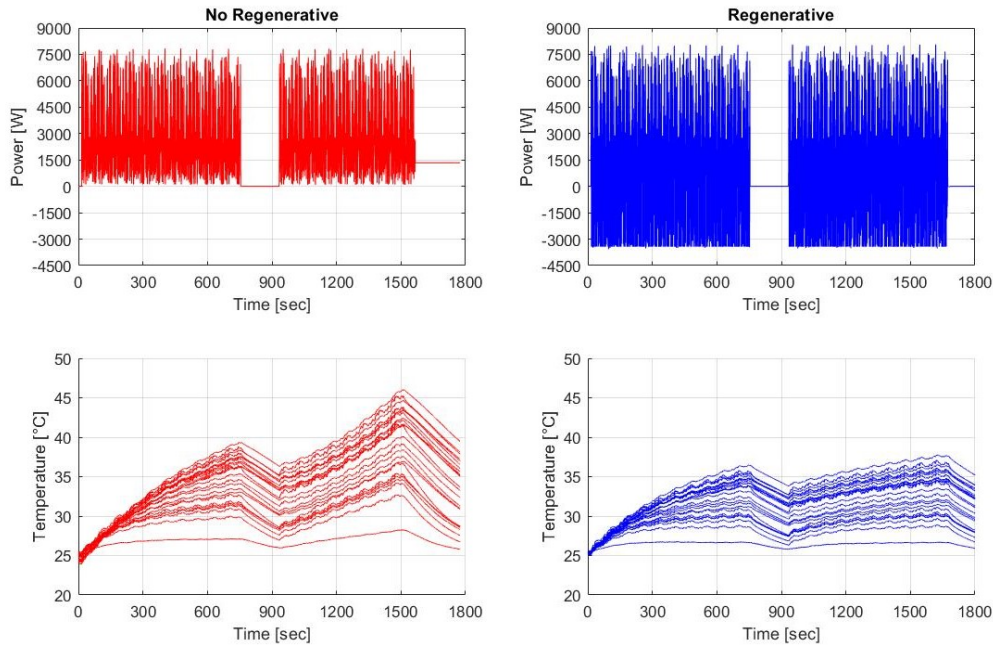


Figure 4.7: Regenerative braking test results

45

## 4.4 Lateral cooling ducts

The lateral cooling ducts were a solution proposed when there was the doubt about a wrong reading of the temperatures. In 2018 the thermistors mounted on the module were placed in grooves obtained in the cells support made of lexan. The support was in contact with the walls of the battery container. The thermistor was hence closed in a small space, near the cells, between the support and the wall. The air could not pass through that point to remove the heat, resulting in a higher temperature with respect to the real cell temperature. A specific test was thought to verify the correctness of this hypothesis.

The test was performed again on a single module inside the thermal chamber described in the previous section (*figure 4.6*). The surrounding temperature was set equal to 25°C. The module was equipped with additional thermistors, as shown in *figure 4.8*, to compare the temperature measured on the cell body with the one measured on the cell pole.

The power profile used for the two tests was again the one obtained from the race of 2018 in Spain. The only difference between the tests was the case used. The first case
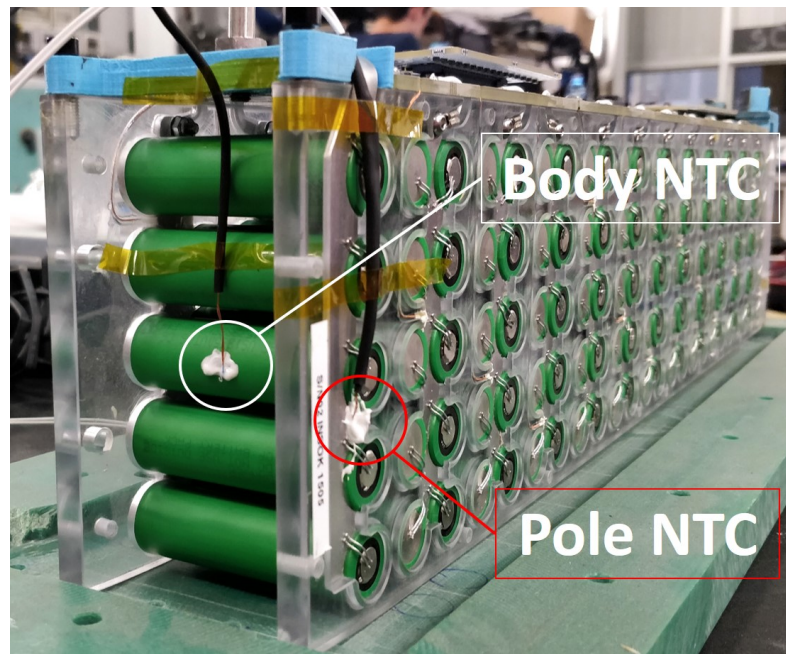


Figure 4.8: Additional thermistors for test
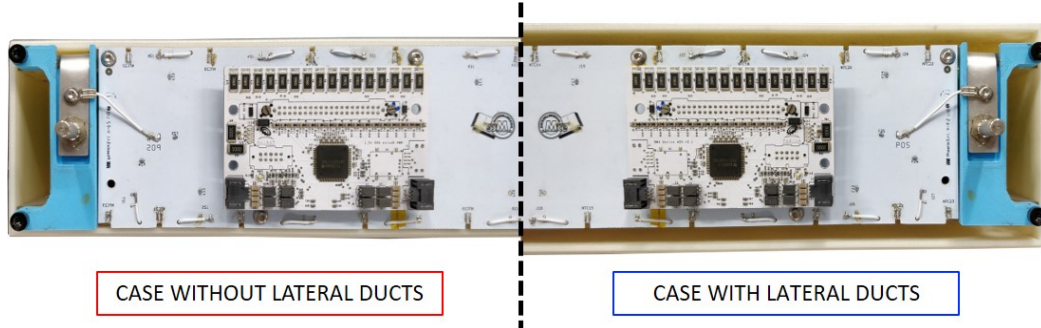
Figure 4.9: Cases used for test

simulated the module without ducts while the second was larger to allow the passage of the air between the cells support and the wall. The two configurations of the case are shown in *figure 4.9*.

In *figure 4.10* are reported the results of the test executed. The temperature versus time graph reports the temperature behaviour of each thermistor mounted on the module.



Figure 4.10: Lateral ducts test results

47

Figure 4.11: Comparison between body and pole temperature

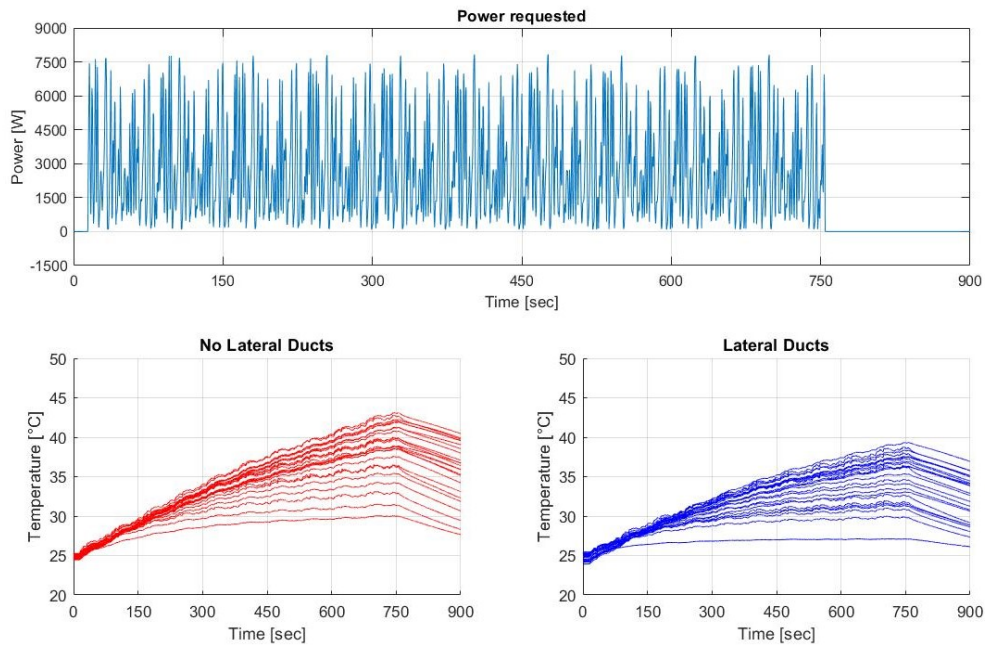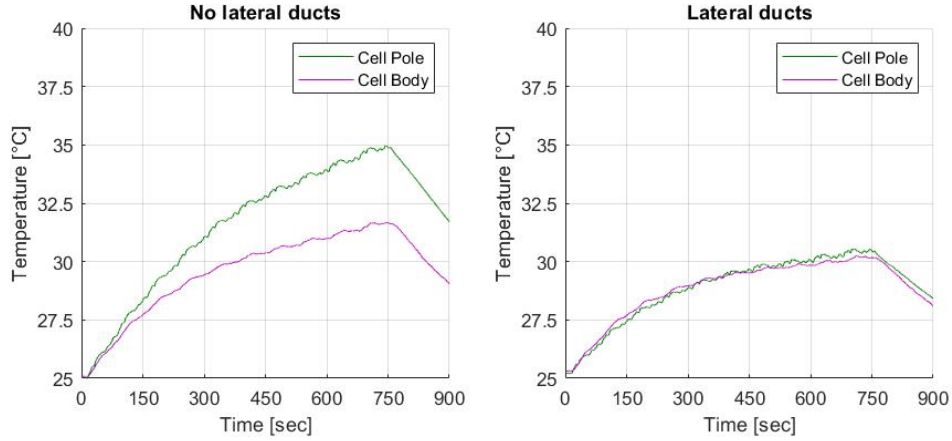The first thing noted was that, with the same power profile, the solution with lateral ducts showed lower temperatures. The difference between the maximum temperature of the two solutions was 3,8°C.

The temperatures registered by the additional thermistors, shown in *figure 4.11*, were of particular interest. In the configuration without lateral ducts the temperature of the pole did not coincide with the one of the body, as it was previously assumed. The two temperatures instead coincided when the case with lateral ducts was used. Moreover, also the body temperature registered was lower with the second case.

The lateral ducts proved to be beneficial for two aspects, they allowed to reduce the temperature and at the same time allowed a correct reading of the cells temperature. For this reason this solution was adopted in 2019.

## 4.5 Vertical spacing of cells

The spacing of the cells is one factor to take into account when dealing with air cooling systems. In choosing it, the trade-off between cooling and space occupied must be taken into account. In general, the thermal behaviour of the air, at the inlet ($T_{in}$) and at the outlet ($T_{out}$), and of the first ($T_{cell,in}$) and last ($T_{cell,out}$) cells, is the one showed in *figure 4.12*. The high difference at the outlet between the air temperature and the cell temperature indicates that the heat exchange is not optimized. The right vertical space can improve this situation.
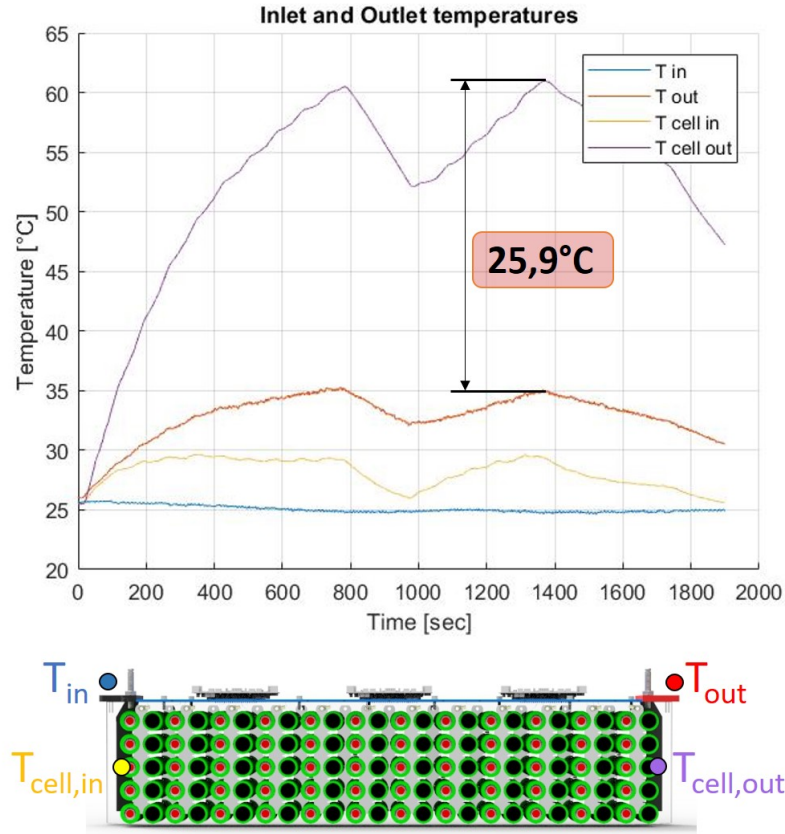
Figure 4.12: Inlet and outlet temperatures

The horizontal space between cells was reduced to the minimum to avoid the battery pack to be too long in the longitudinal direction. The vertical spacing, instead, was chosen taking into account the best trade-off between cooling and vertical obstruction of the battery pack. The maximum space which could be tolerated in vertical direction was equal to 6 mm, due to obstruction of other elements located in the rear compartment.

A CFD analysis was executed to choose the best vertical spacing between cells. The simulations were done for 3, 6 and 9 mm spacing. The results of the simulations are shown in *figure 4.13* and are summarized in *table 4.1*.

(a) *3 mm*



(b) *6 mm*



(c) *9 mm*

Figure 4.13: CFD for optimal vertical spacing

|       | Mass flow rate [kg/s] | Maximum temperature [°C] |
|-------|-----------------------|--------------------------|
| **3 mm** | 0,040 | 46,9 |
| **6 mm** | 0,045 | 41,0 |
| **9 mm** | 0,048 | 39,0 |

Table 4.1: Results of CFD for vertical spacing

The simulations stated that, the higher was the space between the cells the lower was the maximum temperature reached. This conclusion led to the final configuration in 2019 of 6 mm, which was the maximum space available in vertical direction.

The CFD method was validated by discharging the module with a constant current of 45 A. This type of behaviour was much easier to simulate with respect to a discontinuous power profile. The results of the simulation were then compared with the real ones (*Figure 4.14*) to understand whether the parameters used for simulating the thermal behaviour were correct.



Figure 4.14: CFD method validation

The temperature data obtained from simulation showed a good correlation with the real ones.

## 4.6 Thermal tests

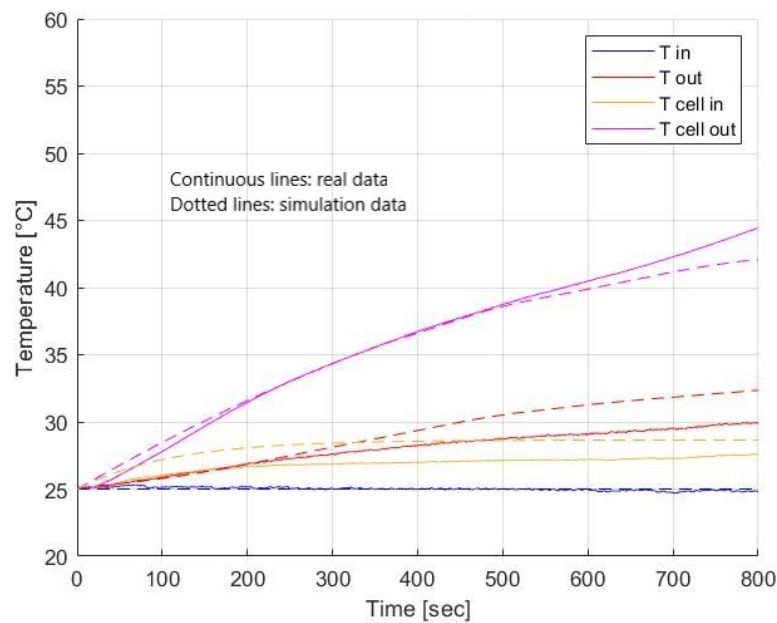The cell chosen in 2019 was equal to the cell used in 2018. However, the selected configuration, regarding number of cells, series and parallels, was different. Despite the difference, it was possible to execute some thermal tests concerning the 2019's configuration by using the 2018's module. It was sufficient to prepare the power profile to be tested, and then to scale it on the old configuration. So, for example, if we wanted to test the response of the cells in the new configuration to 10000 W, it was sufficient to divide that number for the number of cells in the 2019's pack configuration (560 cells) and then multiply it for the number of cells present in the 2018's module configuration (120 cells).

The tests were executed in thermal chamber as explained in the section 4.3. The power profiles were obtained starting from the best lap of the race run in Spain in 2018, repeated 20 times to cover the entire endurance duration. The regeneration power was instead derived from the brake pedal sensor and scaled to obtain a reasonable percentage of regeneration.

In *figure 4.15* and in *figure 4.16* are reported the power profile and the temperature of the two tests performed. The first graph of each figure represents the starting power profile referred to the 2019's pack configuration, while the second one is the power scaled on the 2018's module as described above. The last graph of each figure shows the temperature trend of each thermistor mounted on the module.

Two different strategies were applied to two different tests. In the first case, the power was reduced in the second stint, when the voltage of the battery pack is lower. In the second test, the endurance was divided into four parts, the first one with a higher power and the remainder with decreasing power. Another difference was the starting temperature that for the first test was 35°C while for the second was 25°C to simulate different scenarios. The regenerative power was obtained always starting from the signal of the brake pedal. It was then inserted in the power profile proportionally to the discharge power. The regenerative power was scaled to obtain a reasonable percentage of regeneration.
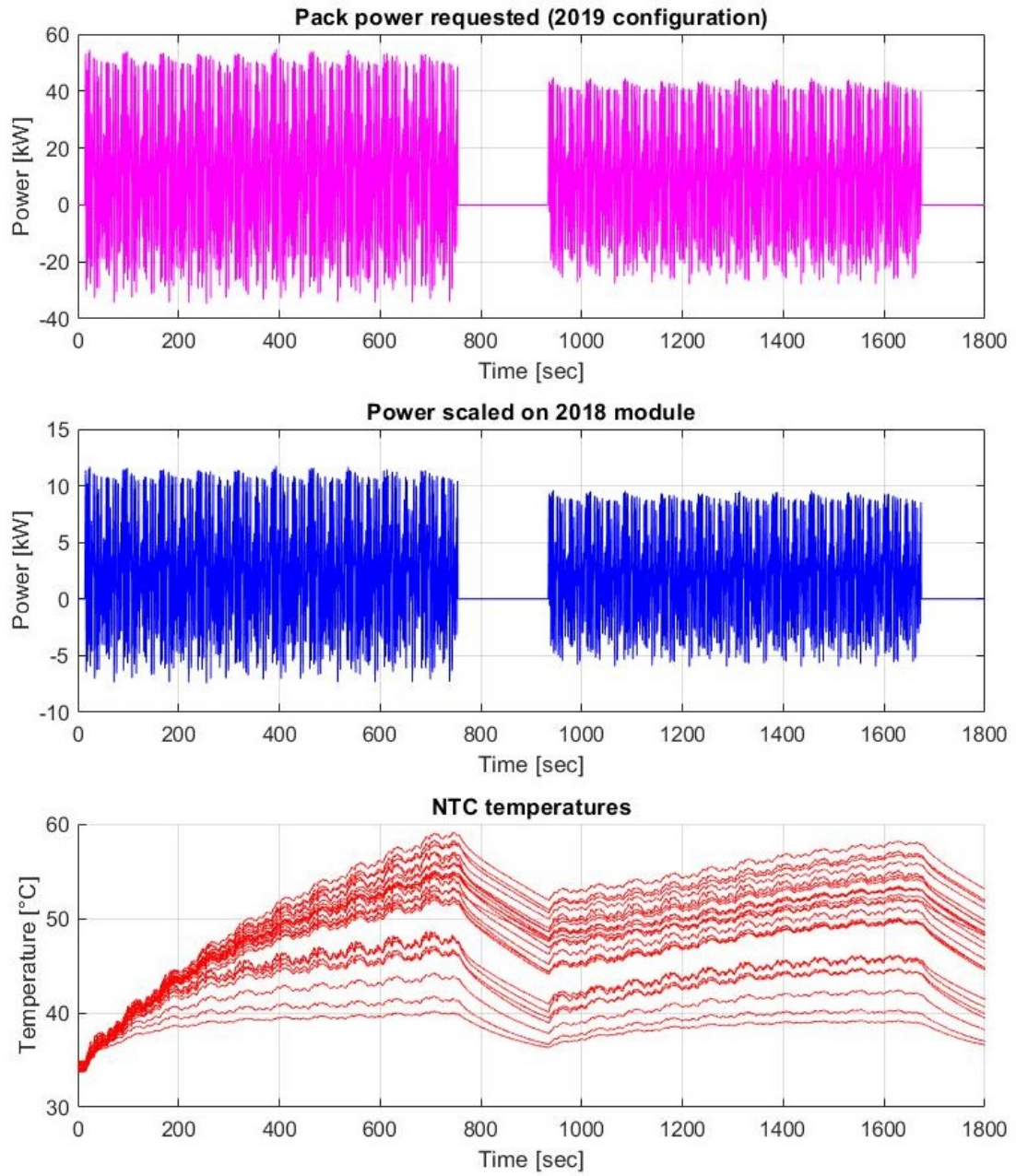
Figure 4.15: First thermal test
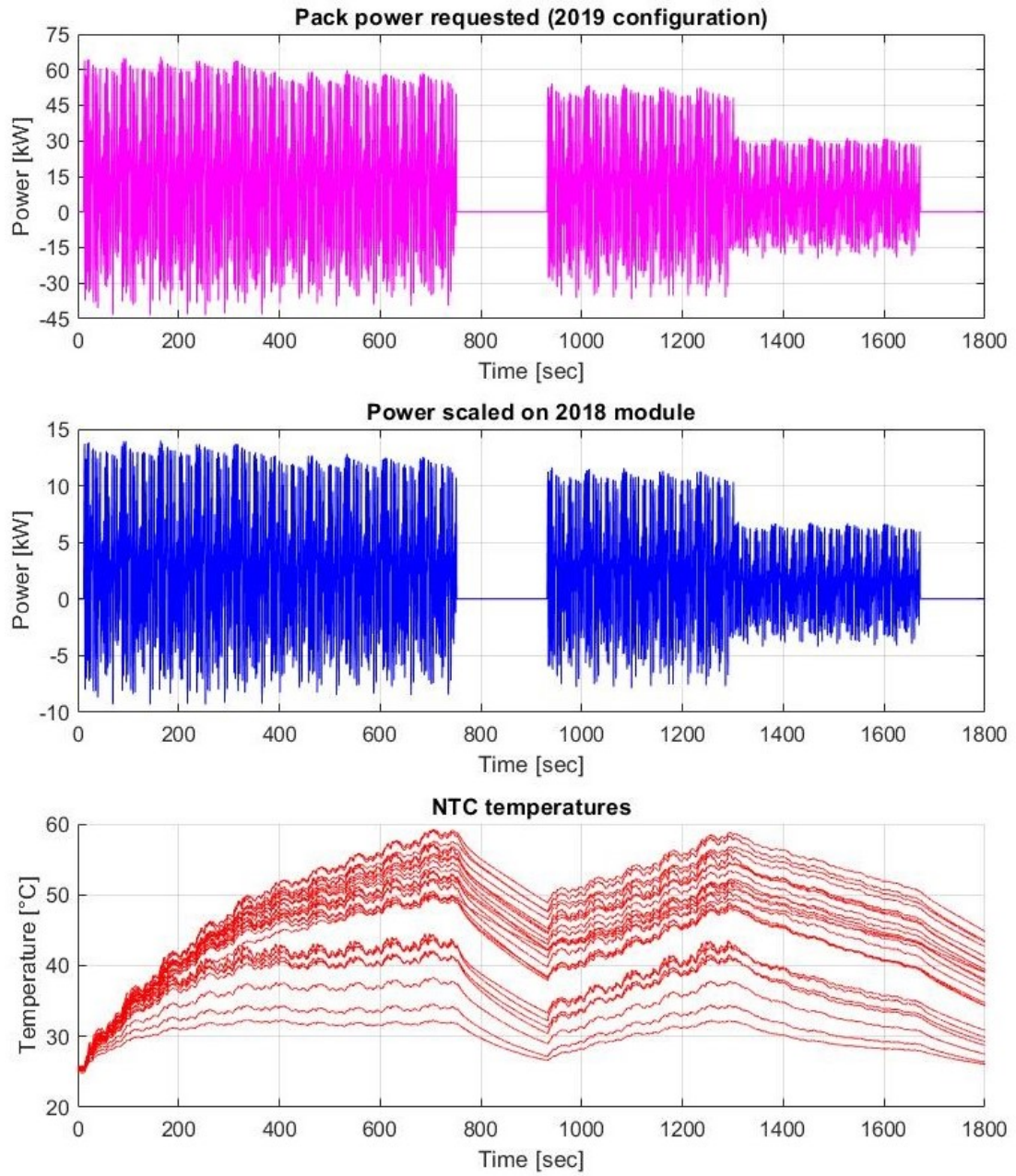
Figure 4.16: Second thermal test

|  | Pack discharge power RMS [kW] | Regenerated energy [%] |
|---|---|---|
| **2018 Spain endurance** | 17,816 | 0,0 |
| **Thermal test 1** | 19,646 | 28,8 |
| **Thermal test 2** | 22,636 | 29,4 |

Table 4.2: Thermal tests properties

In *table 4.2* are reported the RMS of the discharge power and the percentage of regeneration. Both the tests were designed to have a higher RMS with respect to 2018.

From the tests resulted that the chosen configuration for 2019 was, theoretically, suitable to complete an endurance without exceeding the temperature limit of 60°C, running faster than in 2018 thanks to the use of regenerative energy.

# Chapter 5

# Battery pack design

## 5.1 Packaging

The packaging of the 2019's battery pack was similar to the 2018's configuration from a macroscopic point of view but was different in many details due to the improvements introduced.

The 4p-140s configuration was divided in five modules with configuration 4p-28s, connected in series as shown in *figure 5.1*. Radlok connectors were used to electrically connect the modules between them [9]. The segments were then divided by vertical walls electrically insulated.
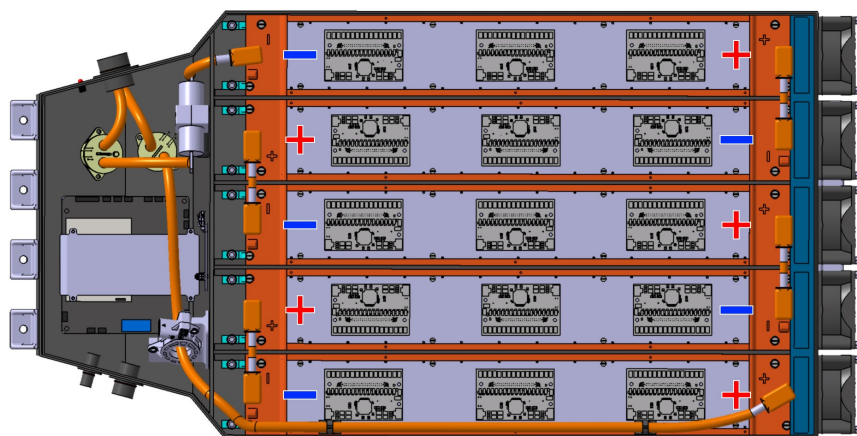
Figure 5.1: Series connection
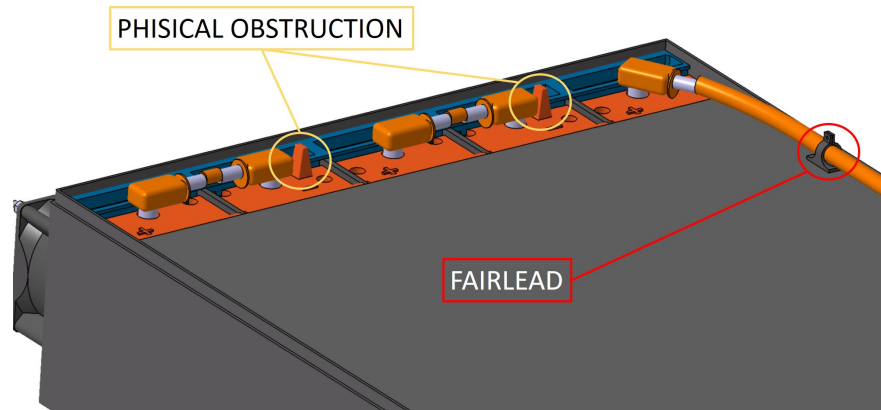
Figure 5.2: Devices for avoiding unintentional connections

The unintentional wrong connection was prevented by the use of simple obstruction elements or fairleads (*figure 5.2*).

The shrinkage of the frontal part of the container was guided by the obstruction of the main hoop. In this part of the battery pack, the following components were positioned:

1. BMS (Battery management system),

2. current sensor,

3. fuse,

4. AIRs (Accumulator Isolation Relays),

5. IMD (Insulation Monitoring Device) board,

6. TSAL (Tractive System Active Light) board,

7. precharge resistance.

The position of each component is illustrated in *figure 5.3* and it was defined into the design phase. They were separated from the modules with an electrically insulated vertical wall. The packaging was maximized by using 3D printed parts. They were used to place the current sensor and the fuse on the vertical wall, and to position the IMD above the BMS to save space.

Figure 5.3: Battery pack frontal part

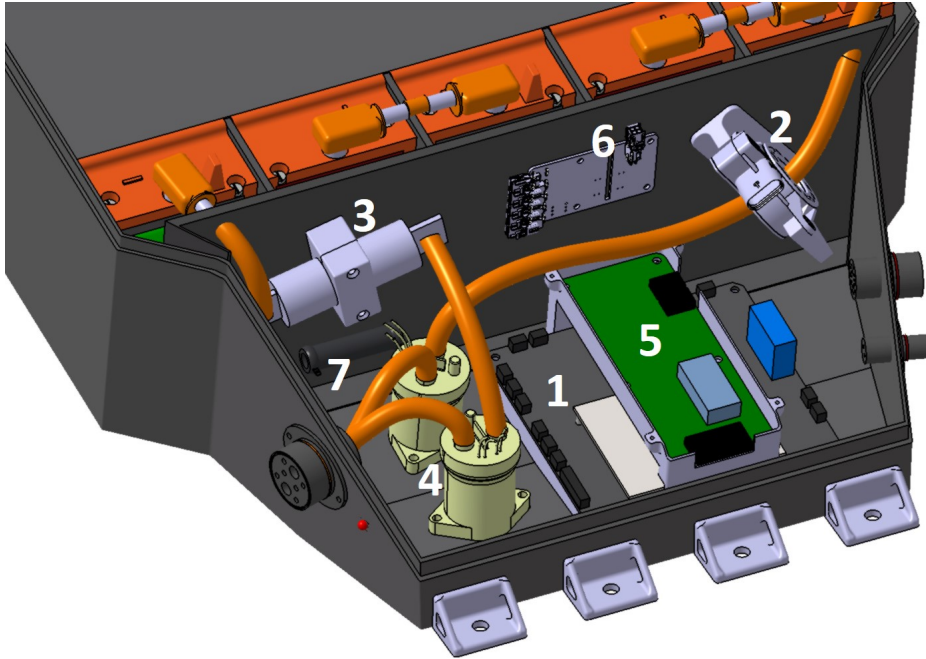The battery pack floor was not planar for its entire length (*figure 5.4*). The angle between the rear part and the frontal part was of 7° to follow the slope of the monocoque. The inclination was guided by the angle of the diffuser, an aerodynamic device used to increase the downforce.
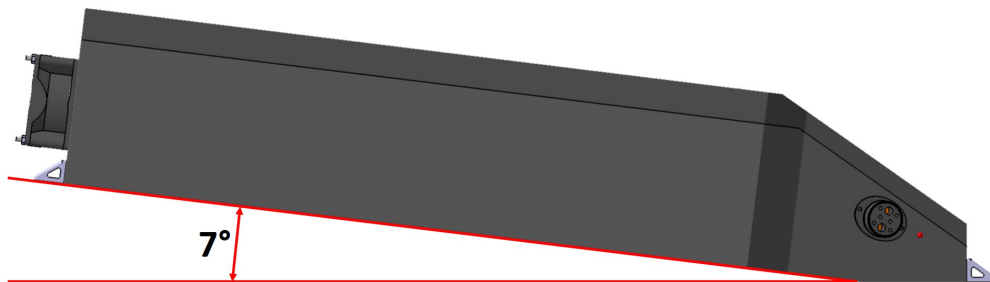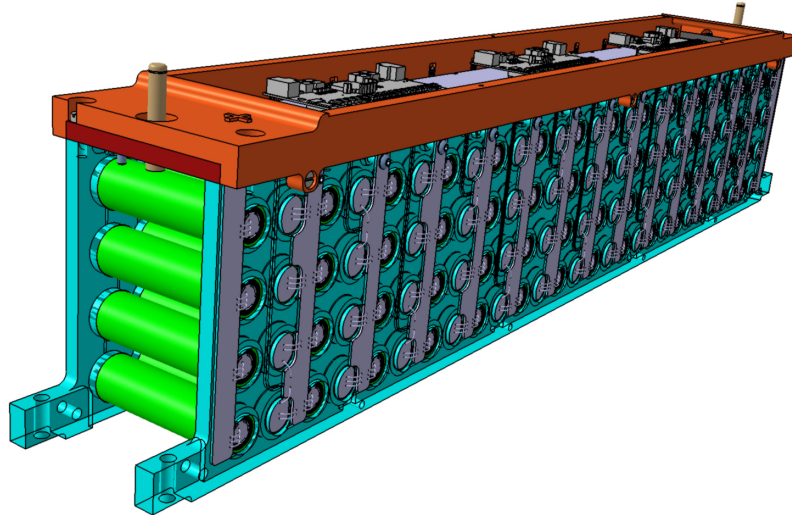


Figure 5.4: Battery pack slope

58

Figure 5.5: 2019's module

## 5.2   Module design

The *figure 5.5* represents the selected configuration for what concerns the module. It was thought to be interchangeable to facilitate the assembly and the maintenance. The 4 parallels were arranged along the vertical direction while the 28 series along the horizontal direction. The electrical connections were done using aluminium busbars as intermediate body. The cells were connected to the busbars by means of aluminium wires using a technology called HWB (Heavy Wire Bonding).

The cells were kept into position by two supports made of Lexan, a material rated UL94V0. This means that the material will not burn for more than 10 seconds after the exposure to a flame. In 2018 the thickness of the support was of 8 mm while in 2019 it was reduced to 6 mm. This was possible thanks to the introduction of the lateral cooling channels, which introduced space to host the wires for electrical connections, that instead were covered by the Lexan in 2018. The thickness reduction reduced the total mass of the cell supports from 2856 g in 2018 to 2280 g in 2019, that is 20,2% weight reduction.

*Figure 5.6* shows the cell support in a more detailed way. The busbars and the NTC thermistors were directly glued on the support in dedicated grooves. In figure are also identified the holes for clamping, needed during milling machine operation, the ones
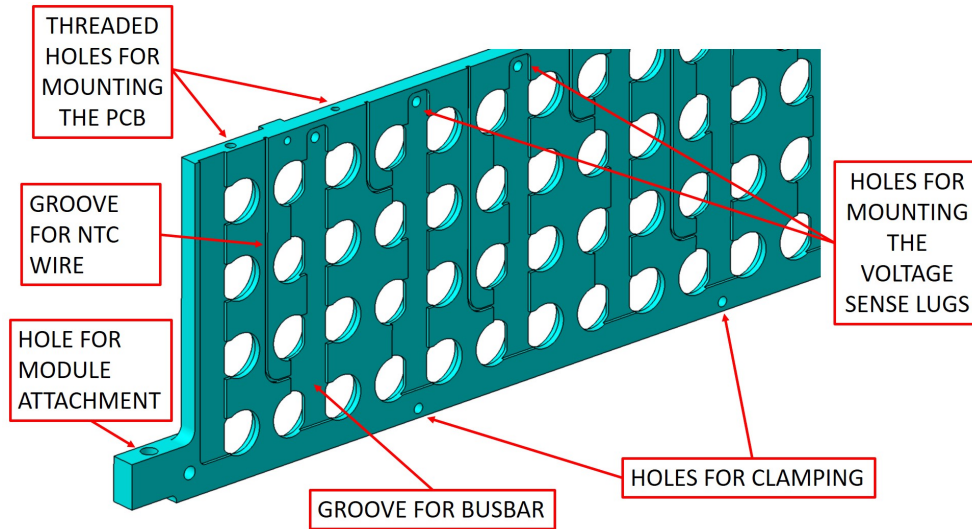
Figure 5.6: Cell support detail

for lugs and PCB mounting, and the one used to attach the module to the accumulator container.

The busbar design was simplified with respect to 2018. The comparison is shown in *figure 5.7*. The geometry simplification allowed to significantly reduce the machining time. The thickness of the busbars in 2018 was 2 mm while in 2019 was 1 mm, and this change helped to reduce the total mass. The busbars weight was reduced of 44,2%, from 654 g to 365 g.
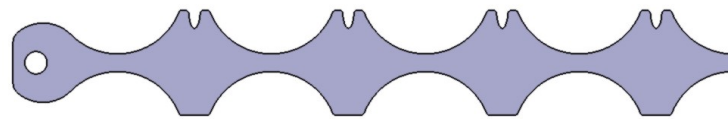


(a) *2018's busbar*



(b) *2019's busbar*

Figure 5.7: Busbars

60
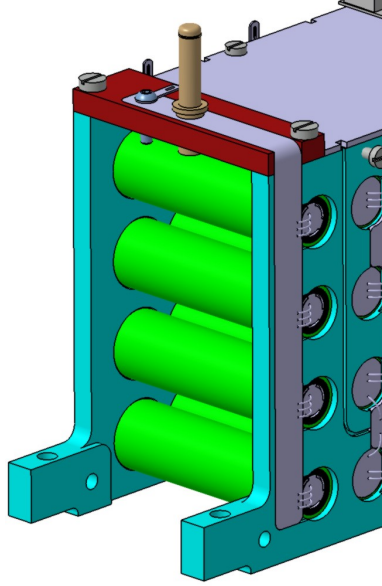
Figure 5.8: Terminal busbar

The thickness reduction affected also the resistance. One busbur had the following measures: 94,2 mm of height, 8 mm of width and 1 mm of thickness. Considering the electrical resistivity $\rho$ of the aluminium, $2.8 \cdot 10^{-8}$ $\Omega$m, and the *equation 5.1*,

$$R = \frac{\rho\, l}{A} \tag{5.1}$$

where $l$ is the length and $A$ is the section, the resistance of one busbar was $2.38 \cdot 10^{-6}$ $\Omega$. Considering all the 145 busbars connected in series, the value of resistance obtained was $3.45 \cdot 10^{-4}$ $\Omega$, which is two orders of magnitude lower with respect to the cell resistance. The resistance increase was therefore considered not enough to affect the power dissipated by heat in a significant way.

The two busbars at the terminal were different from the others (*figure 5.8*). They had a rectangular shape, even simpler than the others because they had not to host NTC thermistors. They were designed longer in order to be tilted on a 3D printed support. A threaded pin was then fastened on the support, in contact with the busbar, using a positive locking nut. The pin represented the negative, or positive, terminal of the module.

The NTC thermistors were placed according to the rules of the competition. They say that the temperature of 30% of the cells must be monitored. A thermistor can also

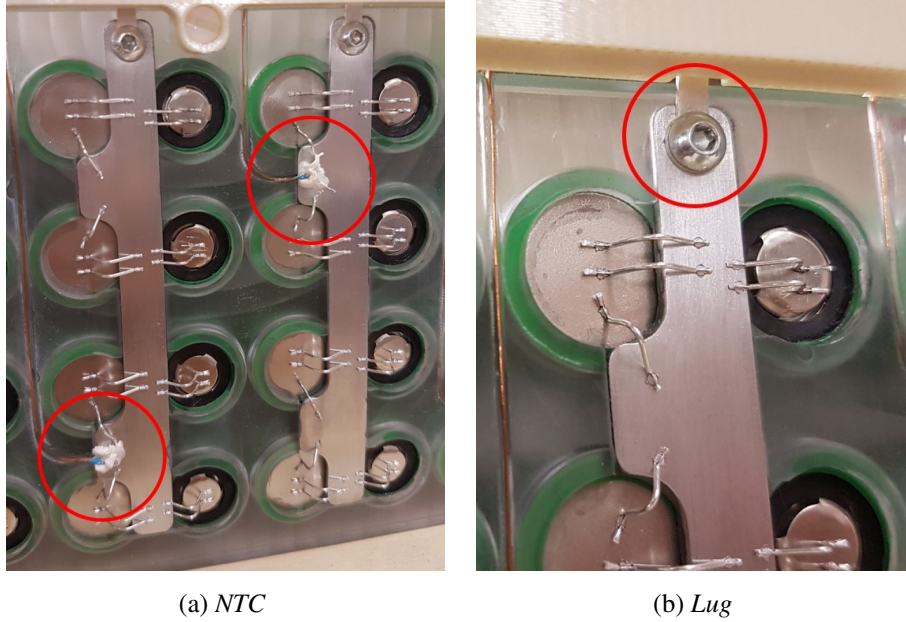(a) *NTC*                    (b) *Lug*

Figure 5.9: Thermistors and sensing voltage lug

be placed on the busbar within 10 mm from the cell negative pole. One thermistor can also monitor more cells if the distance requirement is satisfied.

The position of the thermistors on the busbars is represented in *figure 5.9a*. Each thermistor was able to monitor two cells since the distance requirement was satisfied for both of them. The height of the thermistors was alternated along the module in order to monitor the temperature in a homogeneous way. Each module was equipped with 24 thermistors monitoring 48 cells. The total number of monitored cells was 240 out of 560 cells, i.e. more than the 42%, well above the limit imposed by the rules.

On the busbars were also mounted the lugs for sensing the voltage (*figure 5.9b*). They were mounted using bolts and positive locking nuts to avoid loosening.

The PCB was placed on top of the module, screwed to the cells supports with non-conductive screws made of nylon. It was the interface between the BMS and the sensors mounted on the module. Both the thermistors and the sensing voltage lugs were soldered onto the PCB in specific zones shown in *figure 5.10*. The BMS slaves were connected to the PCB to collect data about temperature and voltage. Each PCB could host three BMS slaves. The PCB had a second function. It was used as a cover for the batteries. In this way, a sort of box was created inside which the air could pass
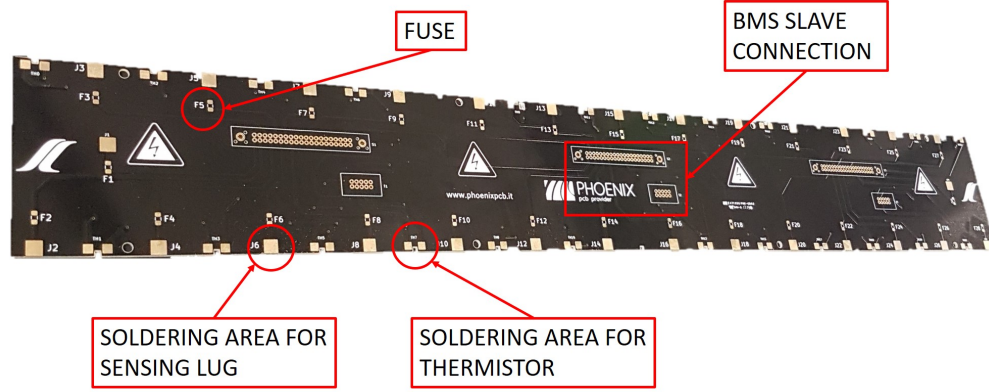
Figure 5.10: PCB

to cool down the cells.

The 3D printed cover, shown in orange in the previous *figure 5.5*, had two functions. It was used as a base to position a cover to protect the PCB from unintentional falling of objects on top of the module that would cause short circuits. The second function was to force a stationary position inside the module container, avoiding the wire bonding to touch the walls and eliminating dangerous vibrations.

The new module packaging allowed to change the design of busbars and cells supports. It resulted in a weight reduction summarized in *table 5.1*.

|  | 2018 | 2019 | Percentage reduction [%] | Weight reduction [g] |
|---|---|---|---|---|
| Cells supports | 2856 g | 2280 g | - 20,2 % | - 576 g |
| Busbars | 654 g | 365 g | - 44,2 % | - 289 g |
| Total |  |  |  | - 865 g |

Table 5.1: New components weight reduction

## 5.2.1 Heavy wire bonding

Nowadays, different technologies exist to join the batteries used in the automotive field [10] [11]. The most economical among them is the resistance welding. It involves localized heating together with pressure to fuse the materials and join them. It

63

provides good automation and quality control. Unfortunately, it is not good for joining aluminium because of its high electrical and thermal conductivity. Moreover, this technology suffers of electrode sticking. Projection welding is a variant of resistance welding in which the heat is concentrated to make the welding process easier. However, this is not the preferred choice when dealing with aluminium.

The laser welding is another solution for joining batteries. It is a non-contact process in which a laser beam is used to heat and melt the materials. It is a very fast and precise process that generates low heat. The laser welding can be affected by the high reflectivity of some materials like the aluminium. The main disadvantage of this process is that it requires zero gap between the parts to be welded. Moreover, being a non-contact process, it is difficult to control the quality of the welding.

The ultrasonic welding uses the energy produced by the ultrasonic vibrations, at 20 kHz or more, to create a solid-state bond between two materials clamped together. It can be used to join dissimilar materials, including copper and aluminium. The heat-affected zone is small, however, the vibrations may cause damage. It needs double-side access, making it suitable especially for pouch cells. Moreover, the surfaces to be joined must be very clean.

The selected technology to join the cells with the busbars fell on the heavy wire bonding. It uses the same concept of ultrasonic welding to weld a wire connecting the battery and the busbar. The HWB has no need for double-side access as in the case of ultrasonic welding and it can therefore be used for cylindrical cells. It presents also the other advantages of ultrasonic welding, i.e. the small heat-affected zone and joining of dissimilar materials. The wires act like fuses that disconnect single cells in case of overcurrent. In addition, when the wire is installed, it is directly tested by the machine to avoid failures. The main disadvantages are due to the clamping method and to the cleaning. The surface to be welded must be well fixed because it has no to vibrate to obtain a good welding result.

The cells were glued to their supports to avoid vibrations and to ensure the correct operation of the HWB. The clamping method was designed according to the models supplied by the service provider. In *figure 5.11* is presented the model used to design the clamping support (green). The grey parts were the components of the machine while the red parallelepiped represented the area of operation. The clamping support had to provide holes for the clamping to the machine and, at the same time, it had
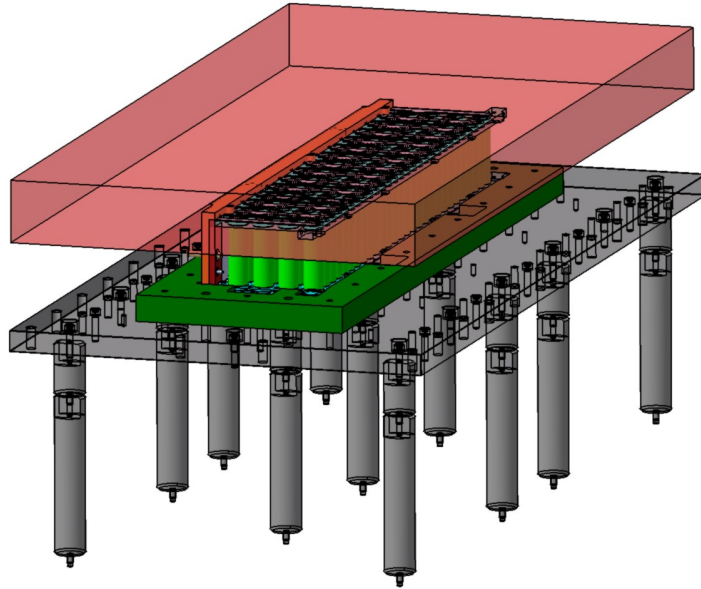
Figure 5.11: Clamping support design



Figure 5.12: Clamping support for HWB application

65

to maintain the module into position using the holes present on the cells support. It was designed considering that the wire bonding was not protected by the cells support, hence, the central part was hollow to allow the module to be turned upside down without ruining the wires. The module placed on the clamping support is shown in *figure 5.12*.

Before the application of the wire bonding, the cell terminals and the busbars were accurately cleaned, firstly with a glass fibre pencil and then by using ethyl alcohol. The final result is shown in *figure 5.13*. The HWB was used in 2018 and it was confirmed in 2019 because of the availability of technology, the ease of automation and the reliability of the solution.
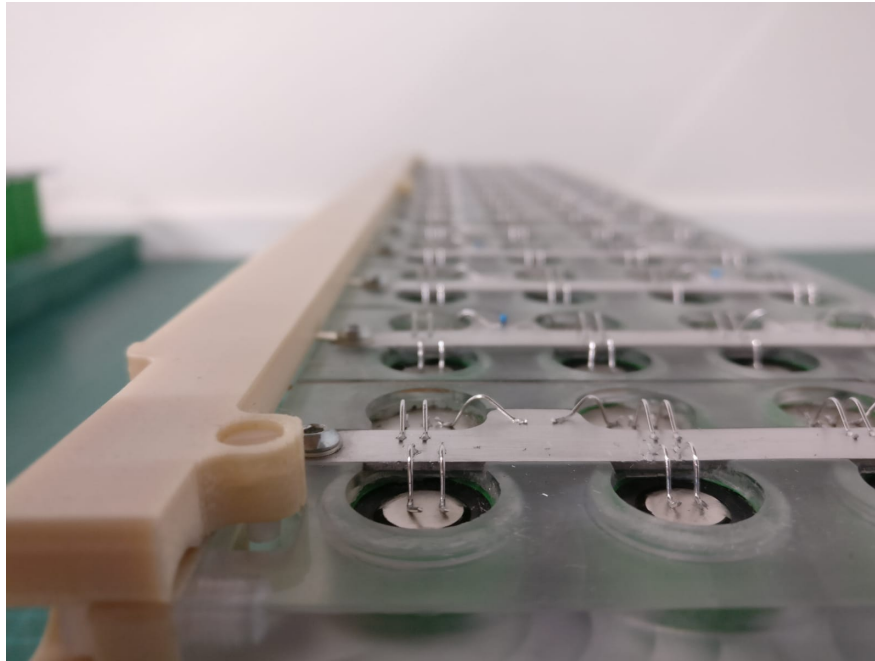


Figure 5.13: HWB detail

## 5.3 Container

The rules about the battery pack container stated that [1]:

*TS accumulator containers must be constructed of steel or aluminium. With the fol-*

*lowing requirements:*

- *The bottom of the accumulator container must be at least 1,25 mm thick if made from steel or 3,2mm if made from aluminium.*

- *The internal and external vertical walls, covers and lids must be at least 0,9 mm thick if made from steel or 2,3 mm if made from aluminium.*

*Alternative materials are allowed with proof of equivalency*

The aluminium and steel were avoided as solutions because of their weight, so an alternative material was chosen. The glass fibre was avoided too because of the low strength-to-weight ratio, despite it had other good properties like the non-electrical conductivity.

The remaining solutions were the Kevlar and carbon fibre. The container of 2018 was made entirely of Kevlar. It guaranteed low weight and dimensions and it did not conduct electricity. It was the best choice from a theoretical point of view but not from the practical one. The manufacturing process resulted very complex, causing waste of time and material. At the end the container resulted good, but the low stiffness was evident.

As in the case of Kevlar, the carbon fibre guarantees low weight. In general, it has lower strength-to-weight ratio than Kevlar, but it has higher stiffness. The main disadvantage of the carbon fibre for battery pack applications is the electrical conductivity. However, it was chosen as material for the 2019's container. It was used in a sandwich version, with honeycomb core reinforcement. The resin used was fire-retardant and the electrical insulation was guaranteed through the use of Kapton tape. The main reason of this choice was the know-how of the team about carbon fibre.

The chosen laminates were then tested to obtain their mechanical properties. The three-point bending test (*figure 5.14a*) was performed to evaluate the flexural modulus and the ultimate tensile strength. The shear test (*figure 5.14b*) was instead aimed at evaluating the shear strength of the laminate.

Two different laminates were used for the container floor and the container walls to meet the requirements established by the rules. The results of the three-point bending tests are shown in *figure 5.15*. The *equations 5.2, 5.3 and 5.4* were used to compute the tensile properties of the laminates.

(a) *Three-point bending*         (b) *Perimeter shear test*

Figure 5.14: Test for mechanical properties

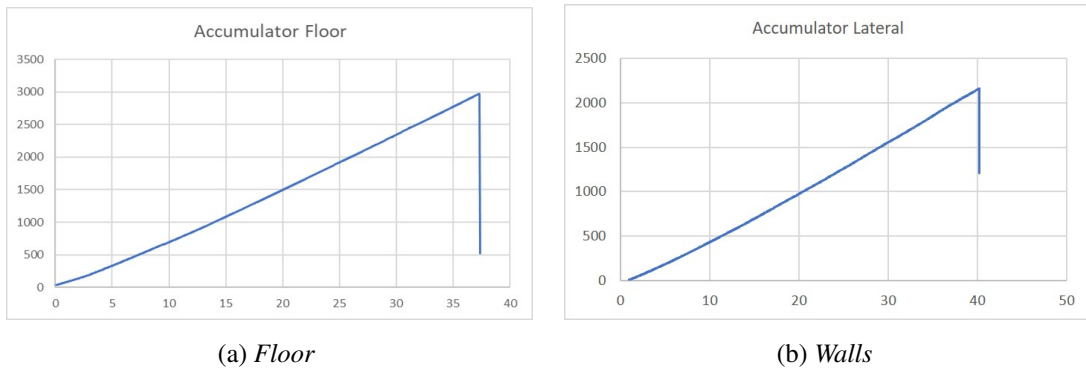

(a) *Floor*         (b) *Walls*

Figure 5.15: Three-point bending results: load [N] vs deflection [mm] curves

$$E = \frac{l^3 G}{48 I} \tag{5.2}$$

$$I = \frac{w t^3}{12} \tag{5.3}$$

$$\sigma_{uts} = \frac{F_{uts} \, l \, t}{8 I} \tag{5.4}$$

Where:

- E: Young's modulus

- $F_{uts}$: maximum force of the force-deflection curve
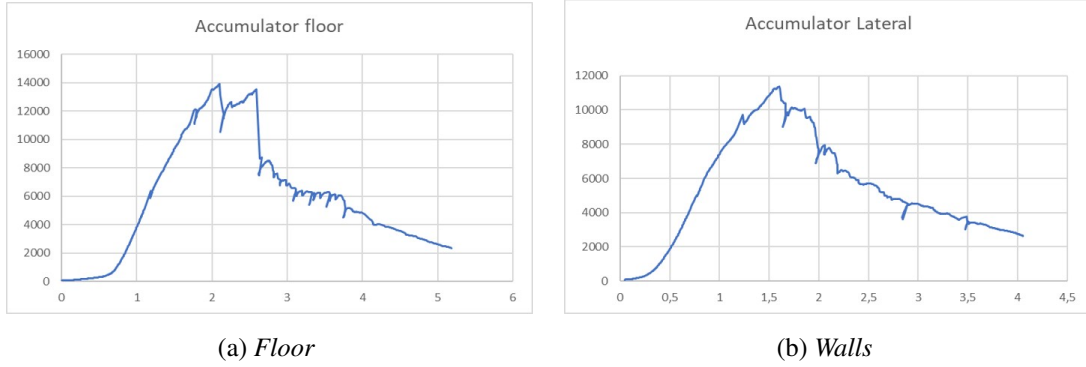
68

(a) *Floor*

(b) *Walls*

Figure 5.16: Perimeter shear test results: load [N] vs deflection [mm] curves

- G: gradient of the force-deflection curve

- I: second moment of area

- l: support span

- t: thickness of the laminate

- w: width of the laminate

- $\sigma_{uts}$: ultimate tensile strength

The results of the perimeter shear test of both laminates are reported in *figure 5.16*. The shear strength of the laminates was computed using the *equation 5.5*.

$$\sigma_s = \frac{F}{\pi D t_1} \tag{5.5}$$

Where:

- D: extruder diameter

- F: force at the peak in which first layer broke

- $t_1$: thickness of upper layer
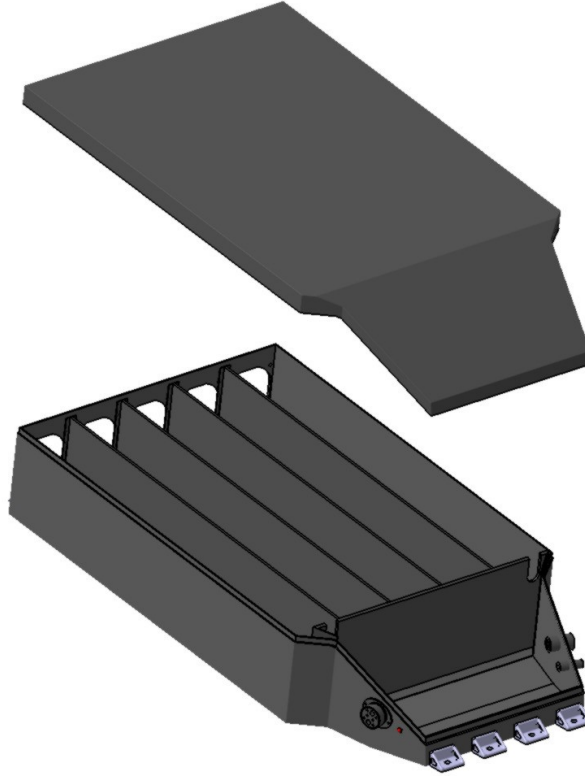
- $\sigma_s$: shear strength

Figure 5.17: Accumulator container and cover

The properties of the laminates obtained through the tests are summarized in *table 5.2*. They were used to demonstrate the equivalence requested by the rules. The cover was made with the same laminate used for the walls. In *figure 5.17* is shown the final shape of the container and the cover.

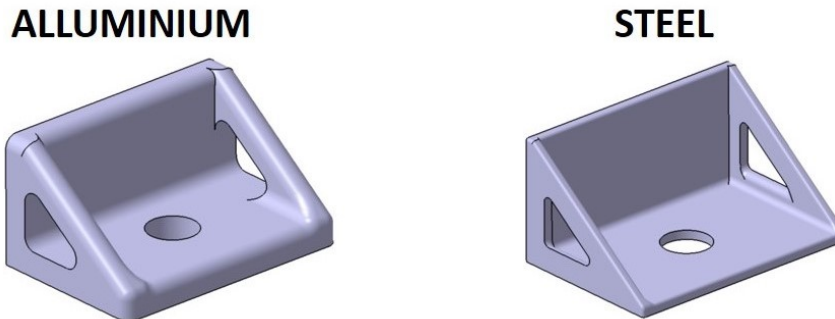|  |  | Floor | Walls |
|---|---|---|---|
| Young's modulus | [GPa] | 49,6 | 69,8 |
| Tensile strength | [MPa] | 318 | 382 |
| Shear strength | [MPa] | 127,7 | 142,2 |

Table 5.2: Laminates properties

Figure 5.18: Brackets comparison

The brackets to mount the battery pack on the car could be made, according to the rules, of steel with a thickness of 1,6 mm or aluminium with a thickness of 4 mm. The shape of the brackets and their comparison is shown in *figure 5.18*. The choice between the two configurations was based on the weight. Despite the major thickness, the aluminium one resulted lighter because of the lower density. It weighted 19,6 g against the 24,5 g of the steel solution.

The brackets were glued to the container with a glue called plexus. It was characterized by shear strength of 26,2 MPa and tensile strength of 27 MPa. The most critical condition was identified in the lateral direction, with the glue loaded in shear. The maximum force admitted was equal to the glued area of 800 mm$^2$, multiplied by the shear strength. Hence, each bracket was able to withstand 20960 N in the lateral direction, which multiplied by 8, that was the number of brackets, resulted 167680 N. The maximum force to withstand, imposed by the rules, was equal to 40 g in the lateral direction. Considering the mass of the battery pack of 39 kg the maximum force exerted was equal to 15303,6 N. By dividing the maximum force allowed with the maximum force exerted, the safety factor obtained was 11.

## 5.3.1 Mould design

The production of carbon fibre components required the design of moulds to obtain the desired shape. The first step was to obtain the shape of the components in the 3D modelling environment as shown in *figure 5.19, 5.20*.

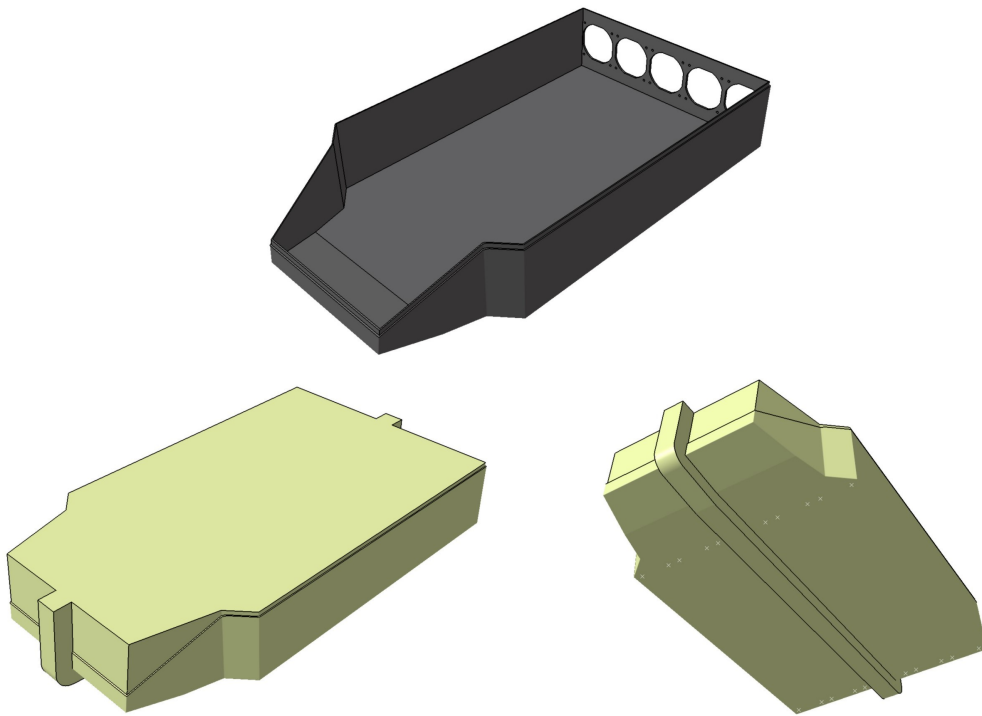The shapes of case and cover were much bigger and more complicated with respect
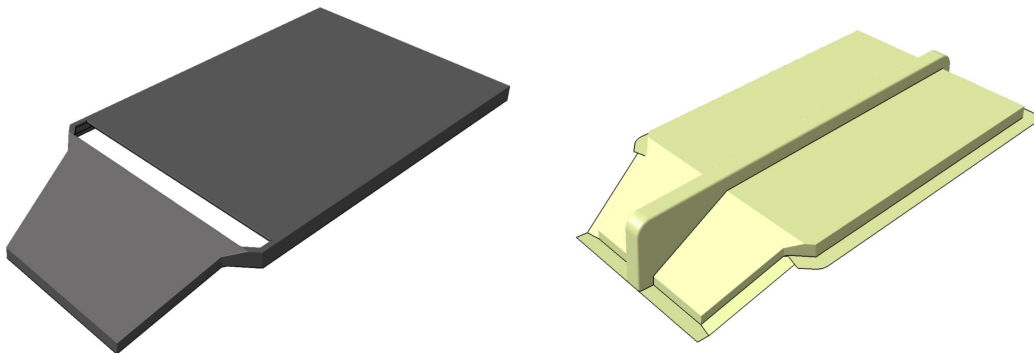
71

Figure 5.19: Case mould



Figure 5.20: Cover mould

to the ones of walls. For this reason, two different methods were used to produce the components.

Typically, when designing a mould, a draft angle is needed to facilitate the extraction of components after curing. In this circumstance, it was not possible to design a draft angle for case and cover because they were designed with perpendicular angles to match perfectly between them and to match also with the modules. A draft angle of the case would have been caused the module cover to not perfectly match the walls, resulting in air leakages and therefore into ineffective cooling. For this reason, the shape of case and cover was firstly obtained and then divided into two specular parts along the longest side. The two parts were then merged adding a sort of separation wall between them.

The shape obtained was then recreated in a resin block, suitable for lamination and cure, by means of a milling machine. At this point, the resin mould was treated according to the following process:

- Correction of defects using a specific plaster.

- Sanding process with increasing grit size until arriving to P800.

- Coating with three layers of sealers, to seal micro-porosity, and three layers of primer, to further reduce the surface roughness to facilitate extraction of carbon fibre components.

Once the resin mould was ready, two semi-moulds were laminated above it as shown in *figure 5.21*. After the curing, two semi-moulds made of carbon fibre were obtained.
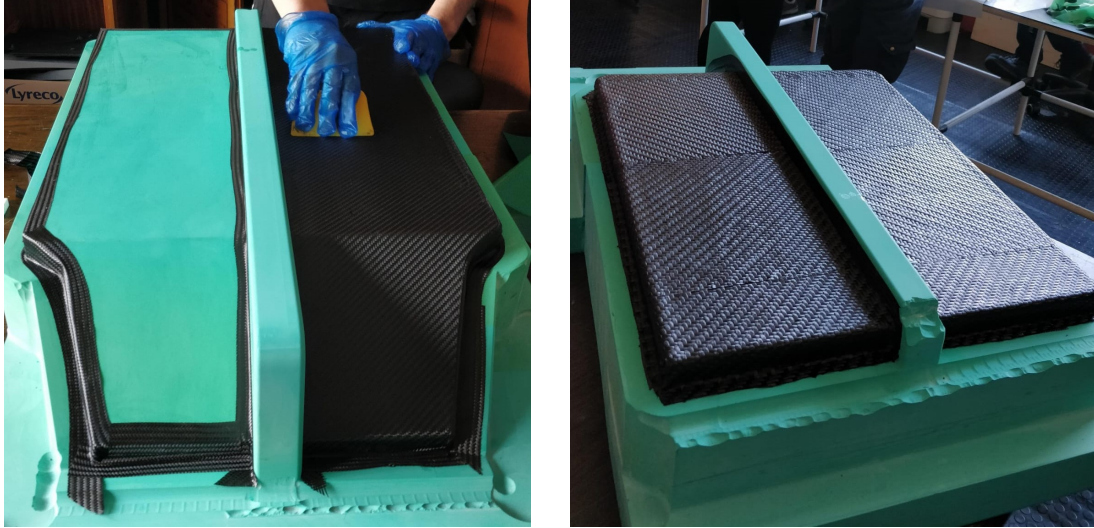
Figure 5.21: Lamination process of carbon fibre moulds

The carbon fibre mould was used as a base to laminate the final component. In figure *figure 5.22* is presented the positioning of the core between the outer and inner carbon fibre skins.
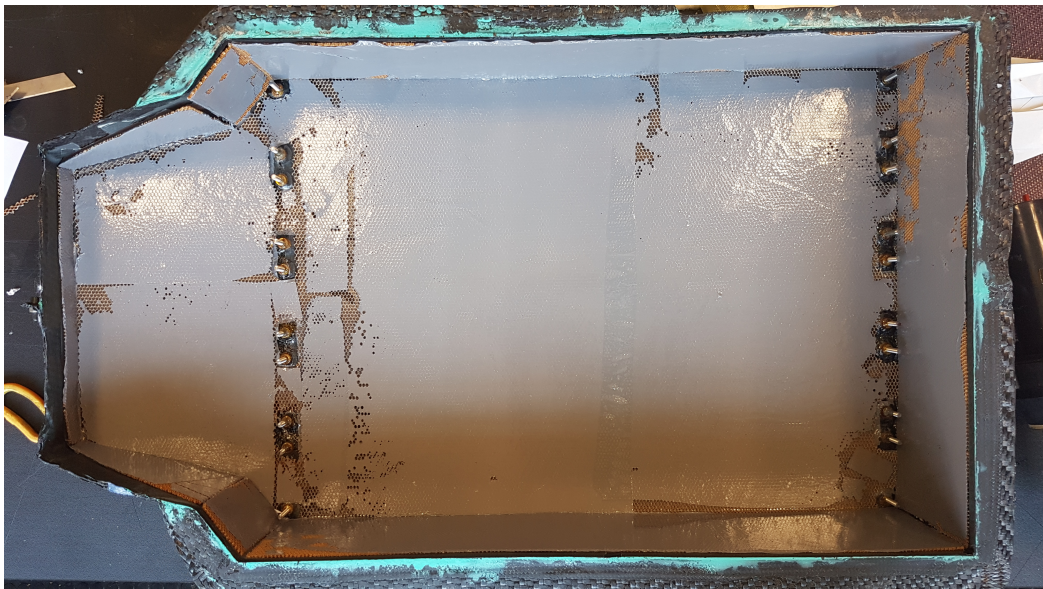


Figure 5.22: Final lamination process

Figure 5.23: Vacuum bag

Before the curing process, the components were closed into a vacuum bag, as shown in *figure 5.23*. The vacuum, together with the pressure built into the autoclave, was used to compress the carbon fibre layers to obtain the desired thickness.

The process to produce the walls was different in some aspects and equal in others. The first step was the definition of the mould shape as shown in *figure 5.24 and 5.25*. The shapes were less complex and the dimensions were smaller. For this reason, the final carbon fibre component was directly laminated above the resin mould, avoiding the intermediate passage which involved the creation of a carbon fibre mould. Also in this case, the resin moulds were obtained through milling and then worked following the process described before. For the vertical walls, the mould was made of two pieces to facilitate the extraction of the component. Both the vertical and the frontal walls were closed in vacuum bags and cured as explained before.
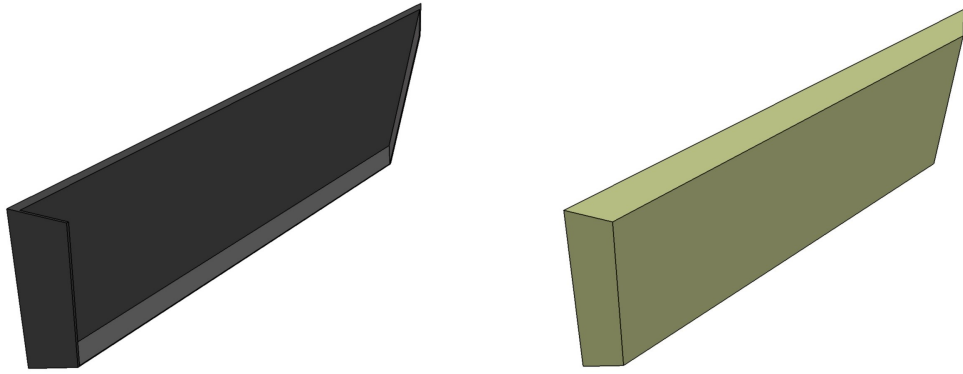
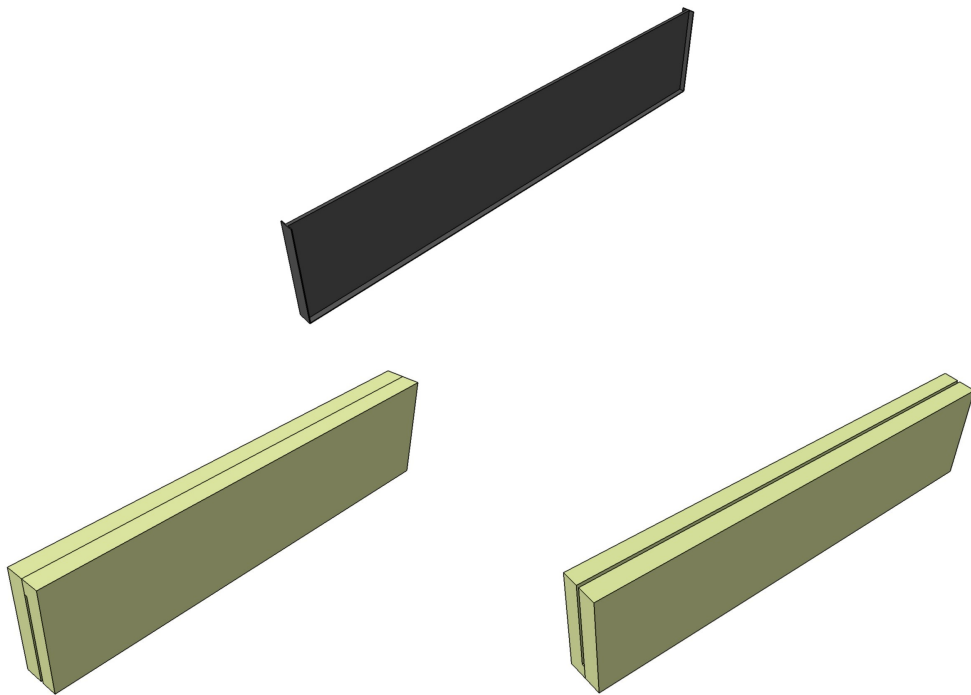Figure 5.24: Frontal wall mould



Figure 5.25: Vertical wall mould

# Chapter 6

# Conclusion and results

The 2019's season began from the analysis of the 2018's battery pack and ended with the production of a new one to mount onto the SC19. The cooling problems emerged during the races push the team to investigate the reason why the battery pack did not perform as in the tests pre-races. Some factors were identified, such as the lack of knowledge about regenerative braking or the absence of a proper intake manifold.

New solutions were implemented while other technologies were confirmed. It was decided at beginning of the season to give continuity to the new battery pack concept introduced in 2018, confirming the Li-ion cells and the HWB technology. The usage of cylindrical cells, characterized by the high density, allowed to build one of the lightest battery pack among the competitors. The result is shown in *figure 6.1, 6.2 and 6.3*.



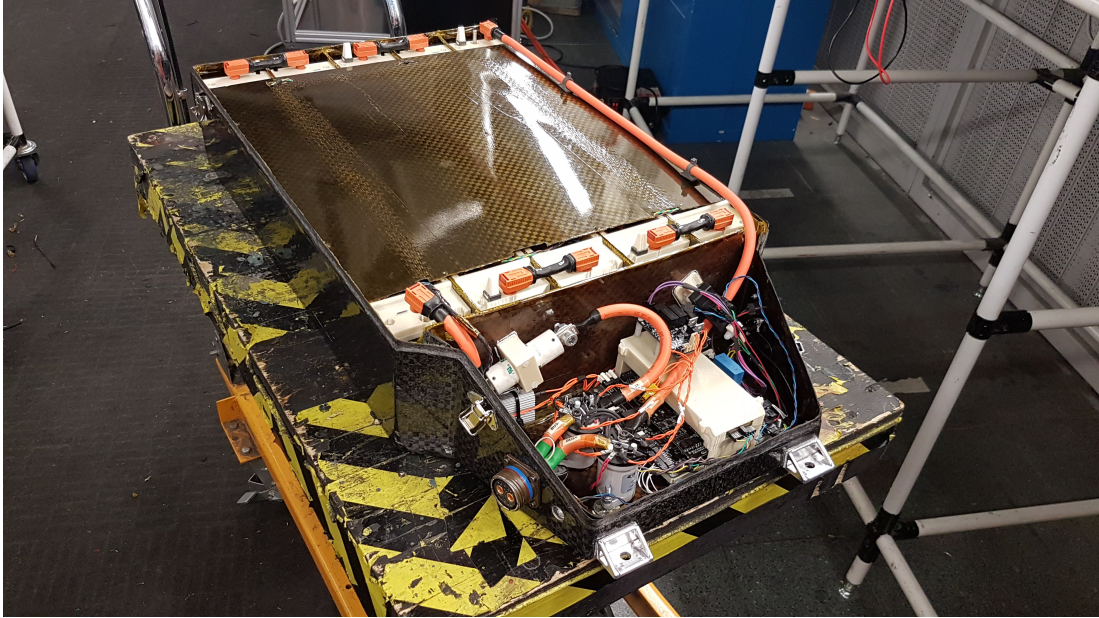Figure 6.1: Module final assembly

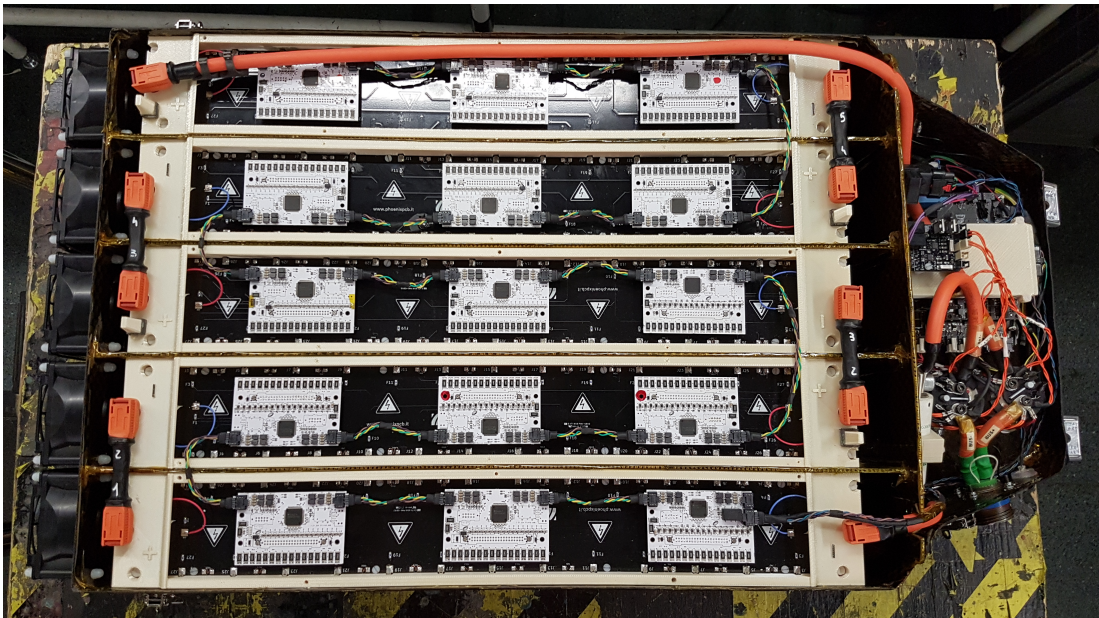Figure 6.2: Battery pack final assembly



Figure 6.3: Top view of the battery pack final assembly

The main target, related to the weight reduction, was the philosophy leading the project. An excellent result was obtained from this point of view. The weight of the battery pack from 2017 to 2019 are summarized in *table 6.1*. From the table is evident the excellent work made by the team through the years, continuously improving to reach the top teams. The reduction of 6,5 kg in 2018 and further 7 kg in 2019 is a stunning result. Together with the weight, also the contribution to the inertia around the vertical axis of the car decreased of 14,8% with respect to 2018, from 13,08 $kg\,m^2$ to 11,14 $kg\,m^2$.

|  | **2017** | **2018** | **2019** |
|---|---|---|---|
| Battery pack weight | 51,8 kg | 45,3 kg | 38,3 kg |
| Weight reduction from 2017 | - | - 6,5 kg | - 13,5 kg |
|  | - | - 12,5 % | - 26,1 % |
| Weight reduction from 2018 | - | - | - 7 kg |
|  | - | - | -15,5 % |

Table 6.1: Weight comparison from 2017

The season ended with the summer races in 2019. The SC19 achieved the first place in the Italian event in Varano de' Melegeri, a historical result for Squadra Corse PoliTo which was the first Italian team to win in the electric vehicles category.

The team participated to other two races, in Czech Republic and Spain, achieving respectively the 6th and 14th place. These results were affected by reliability problems due to the late in car building which resulted in very few hours of track tests.

The battery pack performed well in the Italian endurance, where the rain and the low temperature conditions helped our thermal management. The other two races did not give any feedback for the endurance that was not completed in both the cases due to other problems. The acceleration and skidpad were well faced by the battery pack, without particular problems.

In the future will be important the production of customized inverters and electric motors in order to finally achieve the top teams performances. They will allow a further weight reduction and a different battery pack configuration.

# Acknowledgment

The experience offered by Squadra Corse PoliTo was one of the best of my entire life. Every minute spent in the office, in the garage and on track, working on the SC19, allowed me to write this thesis and to develop skills that I consider fundamental for my future. For this reason, I want to thank Professor Tonoli, supervisor of my thesis and Squadra Corse PoliTo. I want to thank also every single component of the team, in particular, Andrea and Paolo, my colleagues of the Battery Pack division.

I want to thank every friend that I met in the years spent at Politecnico. They truly helped me to face every exam that I sustained.

Thanks to my lifelong friends: Luca, Gianluca and Christian. They are the ones who make my life lighter.

A special thanks to my parents, my sister and the rest of my family. They supported me through my studies, emotionally and economically. I will always be grateful to them.

Finally, my biggest thanks go to my girlfriend Roberta. She encouraged me when I wanted to give up. I would never be able to end my studies without her.

I dedicate this result to all of them. Thank you all.

# Bibliography

[1] SAE International, *Formula student rules 2019*, V.1.1, 2019

[2] S.F. Tie, C.W. Tan, *A review of energy sources and energy management system in electric vehicles*, << Renewable and Sustainable Energy Reviews >>, Vol. 20, pp 82-102, 2013.

[3] T. Martin, R. Burke, *Practical field weakening current vector control calculations for PMSM in vehicle applications*, World Electric Vehicle Symposium and Exhibition (EVS27), pp. 1-7, 2013.

[4] D. Linden, T.B. Reddy, *Handbook of batteries*, Mcgraw-hill, 2001.

[5] T. Sasaki, et al., *Memory effect in a lithium-ion battery*, << Nature Mater >>, Vol. 12, pp. 569–575, 2013.

[6] The Boston Consulting Group, *Batteries for electric cars*, 2010.

[7] Battery University, *Why are protection circuits needed?*, https://batteryuniversity.com/learn/article/safety_circuits_for_modern_batteries [online]

[8] M. Maglio, *Lithium-ion traction battery design for FSAE racing Car*, Rel. Andrea Tonoli, Politecnico di Torino, Corso di laurea magistrale in Automotive Engineering, 2019.

[9] Amphenol, *Radlok connector*, https://www.amphenol.co.jp/military/catalog/RADLOK.pdf [online]

[10] A. Das, et al., *Joining technologies for automotive battery systems manufacturing*, <<World Electric Vehicle Journal>>, 9. 22. 10.3390/wevj9020022, 2018.

[11] S. Lee, et al., *Joining Technologies for Automotive Lithium-Ion Battery Manufacturing: A Review*, ASME 2010 International Manufacturing Science and Engineering Conference, MSEC 2010. 1. 10.1115/MSEC2010-34168, 2010.